

Recursive Soft Drop

Frédéric A. Dreyer,¹ Lina Necib,² Gregory Soyez,³ and Jesse Thaler¹

¹*Center for Theoretical Physics, Massachusetts Institute of Technology, Cambridge, MA 02139, USA*

²*Walter Burke Institute for Theoretical Physics, California Institute of Technology, Pasadena, CA 91125, USA*

³*IPhT, CEA Saclay, CNRS UMR 3681, F-91191 Gif-sur-Yvette cedex, France*

E-mail: fdreyer@mit.edu, lnecib@caltech.edu, gregory.soyez@ipht.fr,
jthaler@mit.edu

ABSTRACT: We introduce a new jet substructure technique called Recursive Soft Drop, which generalizes the Soft Drop algorithm to have multiple grooming layers. Like the original Soft Drop method, this new recursive variant traverses a jet clustering tree to remove soft wide-angle contamination. By enforcing the Soft Drop condition N times, Recursive Soft Drop improves the jet mass resolution for boosted hadronic objects like W bosons, top quarks, and Higgs bosons. We further show that this improvement in mass resolution persists when including the effects of pileup, up to large pileup multiplicities. In the limit that N goes to infinity, the resulting groomed jets formally have zero catchment area. As an alternative approach, we present a bottom-up version of Recursive Soft Drop which, in its local form, is similar to Recursive Soft Drop and which, in its global form, can be used to perform event-wide grooming.

KEYWORDS: QCD, Hadronic Colliders, Standard Model, Jets

Contents

1	Introduction	1
2	The Recursive Soft Drop algorithm	3
2.1	Review of Soft Drop	3
2.2	Introducing Recursive Soft Drop	4
2.3	Dynamic R_0 for aggressive grooming	6
3	Basic properties of Recursive Soft Drop	6
3.1	Groomed radii and momentum fractions	6
3.2	Non-perturbative effects	7
3.3	The $N \rightarrow \infty$ limit of zero-area jets	8
4	Improved mass resolution	10
4.1	Definition of the mass peak and resolution	10
4.2	Two-prong W decays	11
4.3	Three-prong top decays	12
4.4	Four-prong Higgs decays in associated production	12
4.5	Boosted top tagging	13
5	Robust pileup mitigation	14
5.1	Mass resolution with SoftKiller	15
5.2	Mass resolution with the area–median method	17
6	Bottom-Up Soft Drop for event-wide grooming	18
7	Conclusions	20
A	Behavior at fixed order	21
B	Additional pileup studies	23
B.1	W and Higgs mass resolution with SoftKiller	23
B.2	Boosted top tagging with pileup	25

1 Introduction

As the Large Hadron Collider (LHC) collides protons at the highest energies accessible in a laboratory setting, electroweak-scale resonances are routinely produced with transverse momenta far exceeding their rest mass. These highly boosted objects will generate collimated hadronic decays, which are often reconstructed as a single fat jet. Due to the

differences in their radiation patterns, fat jets originating from boosted objects can be distinguished from ordinary quark and gluon jets by studying their substructure. Since the start of the experimental program of the LHC, jet substructure has matured into a highly active field of research [1–7]. First introduced in the pioneering studies of Refs. [8–11], jet substructure was revived by seminal work showing its potential application in the search for a light Higgs boson decaying to bottom quarks [12].

By now, a variety of tools use jet substructure to tag boosted objects and mitigate contamination from poorly modeled contributions such as underlying event and pileup [13–57], which have already found numerous experimental applications [58–94]. One particular technique that has emerged both as a powerful substructure probe and as an analytically tractable approach is the modified Mass Drop Tagger (mMDT) [28], and its later extension, Soft Drop (SD) [42]. The SD procedure takes an initial jet with radius R_0 , reclusters its constituents with the Cambridge/Aachen (C/A) algorithm [95, 96], and removes soft wide-angle emissions that do not satisfy the SD condition, defined as

$$\frac{\min(p_{t,1}, p_{t,2})}{p_{t,1} + p_{t,2}} > z_{\text{cut}} \left(\frac{\Delta R_{12}}{R_0} \right)^\beta, \quad (1.1)$$

where the notation will be reviewed below. This method has been used in a variety of analyses at the LHC, including jet mass and transverse momentum measurements in dijet events [97, 98], vector resonance and dark matter searches [99–102], and boosted $H \rightarrow b\bar{b}$ searches [103]. It has also been used as a powerful probe of the QCD splitting function, both in proton-proton collision [104, 105] and in heavy ion collisions [106–108], where the shared momentum fraction z_g provides a handle on medium effects [109–111]. Because grooming with mMDT/SD removes complications due to unassociated wide-angle emissions, it has also allowed analytic calculations of the groomed jet mass to reach unprecedented accuracies [50, 51, 54, 55].

In this paper, we introduce a recursive extension of the SD algorithm—aptly named Recursive Soft Drop (RSD)—where SD is reapplied along the C/A clustering history until a specified number N of SD conditions have been satisfied. We focus on jet grooming with RSD, taking an angular exponent $\beta \geq 0$. The case $N = 0$ involves no jet grooming, the case $N = 1$ corresponds to the original SD procedure, and the cases $N \geq 2$ are well-suited to multi-prong boosted objects. Like the original SD, RSD is stable under hadronization and underlying event effects, but RSD is able to provide improved jet mass resolution for signals such as boosted 2-prong W bosons, 3-prong top quarks, and 4-prong Higgs bosons. Intriguingly, in the $N \rightarrow \infty$ limit, groomed jets from RSD formally have zero catchment area [112], a feature that suggests that RSD would be well suited for pileup mitigation.

We focus our attention here on the phenomenological applications of RSD, leaving a detailed study of its analytical properties to future work. The behavior of RSD is summarized in Fig. 1 in the case of distinguishing boosted top quark signals from quark/gluon jet backgrounds. As the number of RSD layers increases, the top mass peak is better resolved, with the best performance (for this choice of SD condition) achieved in the infinite N limit, hereafter labeled RSD_∞ . For quark/gluon jets, RSD has a much smaller impact on the groomed mass, but there are still substantial gains in top tagging performance just

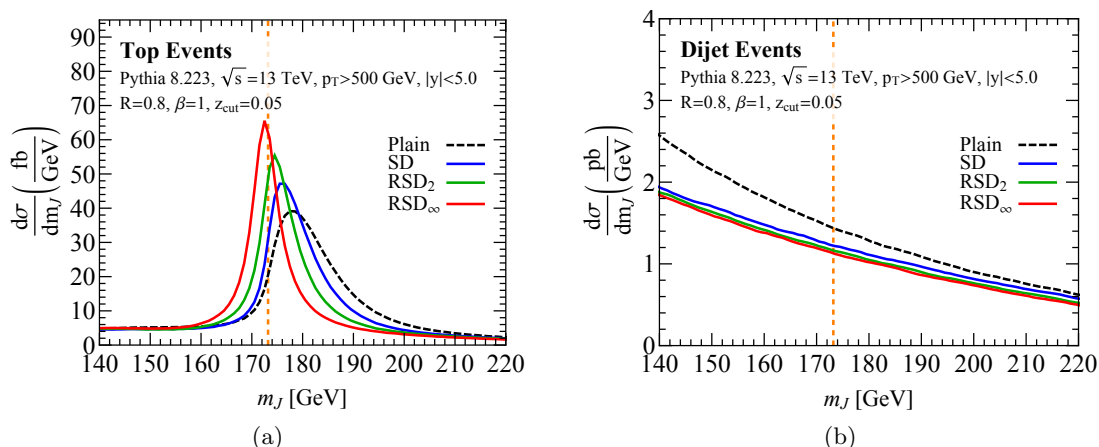


Figure 1. Behavior of RSD in (a) boosted top signals and (b) corresponding dijet backgrounds, using PYTHIA 8.223 and $R = 0.8$ anti- k_t jets. The benchmark SD condition in Eq. (1.1) uses $\beta = 1$ and $z_{\text{cut}} = 0.05$.

from the increased signal mass resolution. In general, any application at the LHC suitable for SD is also suitable for RSD, with the possibility of loosening the SD condition while increasing the number of layers N to balance performance and robustness. As a concrete example, we show how to use RSD_∞ in combination with either the SoftKiller [113] or the area-median method [112, 114] to mitigate pileup in high-luminosity conditions.

The rest of this paper is organized as follows. We introduce the RSD algorithm in Sec. 2, and describe its basic features in Sec. 3, such as its robustness to non-perturbative effects and the $N \rightarrow \infty$ limit of zero-area jets. In Sec. 4, we show how RSD improves jet mass resolution for boosted resonances with hadronic decays, and we present a brief case study of boosted top tagging. In Sec. 5, we discuss the application of RSD to pileup mitigation. We present an alternative version of the RSD algorithm in Sec. 6, where a bottom-up strategy can be applied locally (at the jet level) or globally (at the event level). We conclude in Sec. 7, leaving additional studies to the appendices.

2 The Recursive Soft Drop algorithm

Since RSD is a generalization of SD, we first summarize the SD algorithm [42] in Sec. 2.1, and introduce the multi-layer RSD_N algorithm in Sec. 2.2. We present a more aggressive RSD variant in Sec. 2.3. Like all jet grooming procedures, RSD_N removes wide-angle soft radiation within a jet, with the new feature that the meaning of “wide angle” is determined recursively.

2.1 Review of Soft Drop

The original SD algorithm starts from any jet, where the constituents are reclustered into a C/A angular-ordered tree [95, 96]. The degree of jet grooming depends on two parameters: the minimum energy fraction z_{cut} allowed for the softer branch, and an angular exponent

β defining how much collinear radiation is removed by the grooming procedure. It is also convenient to introduce a reference angular scale R_0 (absorbable into the definition of z_{cut}), which is typically set to the initial jet clustering radius R . We denote by $p_{t,i}$ the transverse momentum of the i -th subjet, and by ΔR_{ij} the rapidity-azimuth distance between the i -th and j -th subjets.

The SD algorithm proceeds as follows:

1. Undo the last C/A clustering step of the jet j and label the two parent subjets as j_1 and j_2 .
2. If these subjets pass the SD condition,

$$z_{12} > z_{\text{cut}} \left(\frac{\Delta R_{12}}{R_0} \right)^\beta, \quad z_{12} \equiv \frac{\min(p_{t,1}, p_{t,2})}{p_{t,1} + p_{t,2}}, \quad (2.1)$$

then the procedure stops and the SD jet j is returned.

3. Otherwise, the softer subjet (by p_t) is removed and the algorithm iterates on the new jet j defined by the harder subjet.
4. If j has no further subjets, either terminate without returning a jet (tagging mode) or define j to be the SD jet (grooming mode).

As explained in Ref. [42], this algorithm is infrared and collinear (IRC) safe for $\beta > 0$ in grooming mode, though it remains Sudakov safe [115, 116] for $\beta \rightarrow 0$.¹ The limits $z_{\text{cut}} \rightarrow 0$ or $\beta \rightarrow \infty$ return an ungroomed jet. Finally, the limit $\beta \rightarrow 0$ corresponds to mMDT [28].

2.2 Introducing Recursive Soft Drop

As depicted in Fig. 2, RSD_N grooms a jet by applying N layers of SD declustering, iterating through the full jet clustering tree. This is achieved by ordering all branches by the ΔR_{ij} separation of their constituents, and iterating through the tree structure by taking the branch with the most widely-separated constituents at each step.

More explicitly, starting from a C/A-reclustered jet:

1. Set the list of branches to a single element: the initial jet.
2. Take the remaining branch whose two parent subjets have the widest separation in ΔR , and label these j_1 and j_2 .² Remove that branch from the list of branches.
3. If the two subjets pass the SD condition in Eq. (2.1), keep both subjets as new branches; otherwise, remove the softer of the two subjets and keep the hardest as a new branch.

¹In tagging mode, SD is IRC safe for $\beta < 0$. If a non-trivial mass cut is applied, SD is also IRC safe in tagging mode for $\beta = 0$.

²During the first iteration, this step is of course trivial, since there is only one branch to the C/A tree.

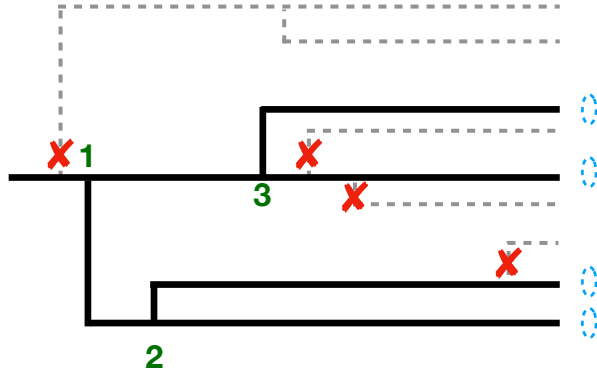


Figure 2. Schematic depiction of the RSD_N algorithm, where a C/A clustering tree is declustered until Eq. (2.1) is satisfied N times. For $N \leq 3$, the grooming stops at the numbered branch N , such that $N = 1$ corresponds to the original SD algorithm. The grooming of all dashed gray lines is achieved for $N > 3$.

4. Iterate this process until the SD condition in Eq. (2.1) has been met N times, or until the C/A tree has been fully recursed through (using the same definitions of grooming/tagging mode as in ordinary SD). The groomed jet is then made of all the remaining branches.

After N iterations where the SD condition is satisfied, one obtains a groomed jet constructed of $(N + 1)$ subjects.³ For $N = 0$, this procedure returns the initial ungroomed jet, while for $N = 1$ it is equivalent to the original SD algorithm. We use $\text{RSD}_N(\beta, z_{\text{cut}})$, or simply RSD_N , to denote RSD grooming with N iterations and parameters β and z_{cut} , such that $\text{RSD}_0 = 1$ and $\text{RSD}_1 = \text{SD}$. For fully recursive SD grooming with $N = \infty$, we use RSD_∞ .⁴

In this paper, we only study RSD with $\beta \geq 0$ in grooming mode. In principle, one could also use $\text{RSD}_N(\beta < 0, z_{\text{cut}})$ to define an $(N + 1)$ -prong tagger. For example, one could use RSD_2 with $\beta < 0$ as a top tagger, much in the way $\text{SD} = \text{RSD}_1$ can be used for boosted W tagging (see Section 7 of Ref. [42]). Ultimately, though, we find that RSD_∞ (with $\beta \geq 0$ in grooming mode) shows good overall tagging performance, making it our recommended default algorithm.

It is worth noting that RSD bears some resemblance to the Iterated Soft Drop (ISD) procedure recently introduced in Ref. [117] for quark/gluon discrimination. A key difference, however, is that RSD follows both branches of the clustering tree, while ISD limits itself to traversing only the harder branch. Both RSD and ISD, along with mMDT and SD, are implemented in `RecursiveTools` ($\geq 2.0.0$) included as part of `fastjet-contrib` [118].

³Alternatively, one could consider a fixed-depth recursion instead, where the SD condition is applied N times on each branch of the clustering tree, resulting in (up to) 2^N prongs. This coincides with the variable depth algorithm in the $N \rightarrow \infty$ limit, but will differ at finite N due to the removal of small angle emissions on the subleading branch.

⁴Note that RSD_∞ is only well defined in grooming mode, and, therefore, only IRC safe for $\beta > 0$.

2.3 Dynamic R_0 for aggressive grooming

In the default RSD algorithm, the R_0 in Eq. (2.1) is fixed to the initial jet radius (henceforth denoted *fixed* R_0 mode). One can instead take a more aggressive approach, in which one updates R_0 dynamically during the grooming procedure.

In this *dynamic* R_0 mode, at each step of the process where two particles i, j meet the SD condition, the R_0 value is updated to $R_0 = \Delta R_{ij}$, with R_0 being kept independent on each branch of the C/A clustering tree. By decreasing R_0 in each grooming step for $\beta > 0$, one imposes a more stringent requirement on the momentum fraction. This yields a more aggressive grooming strategy for all $N > 1$.

For most practical purposes, the dynamic R_0 variant behaves quite similarly to RSD with a smaller β value. As we will see in Sec. 5.2, though, it does have some specific advantages for pileup mitigation with area–median subtraction.

3 Basic properties of Recursive Soft Drop

We perform a variety of parton shower studies in this paper to highlight the features of RSD. In this section, as well as in the more detailed studies in Secs. 4 and 5, we always generate $\sqrt{s} = 13$ TeV proton-proton collisions in PYTHIA 8.223 [119–121] with the default 4C tune. To reduce computation time, we turn off π^0 and B -hadrons decays (still letting other hadrons decay).⁵ Jet clustering is performed with FASTJET 3.2.1 [123], using the anti- k_t algorithm [124] with the default E -scheme recombination and a jet radius $R = 0.8$. We then select jets that have transverse momentum $p_T > 500$ GeV and rapidity $|y| < 5$.

To demonstrate the key similarities and differences between SD and RSD_N , we discuss the groomed radii and splitting scales in Sec. 3.1, the robustness to non-perturbative effects in Sec. 3.2, and the $N \rightarrow \infty$ limit of zero-area jets in Sec. 3.3. In App. A, we present fixed-order studies of the RSD jet mass distribution to order α_s and α_s^2 .

3.1 Groomed radii and momentum fractions

In addition to grooming a jet, RSD defines a range of new jet observables. At each SD step i , one can define the groomed radius $R_{g,i}$ and momentum fraction $z_{g,i}$, equal to the ΔR_{12} and z_{12} values for the corresponding branch that passes Eq. (2.1). For $\beta > 0$, the $R_{g,i}$ observables are IRC safe, while the $z_{g,i}$ are in general Sudakov safe [116]. Thus, after N layers of RSD grooming, we obtain N pairs of $\{R_{g,i}, z_{g,i}\}$ values containing information about the grooming history of the jet. The values obtained for $i = 1$ are identical to the ones obtained from ordinary SD.⁶

We now consider boosted top quark events from the process $pp \rightarrow t\bar{t}$, forcing the tops to decay in the hadronic channel. In Fig. 3a, we show the $R_{g,i}$ distributions from RSD_i with $i \in \{1, 2, 3, 4\}$, taking $\beta = 1$ and $z_{\text{cut}} = 0.05$ as baseline parameters. As expected, the

⁵One might wonder whether π^0 and B -hadrons decays would affect our SoftKiller pileup study in Sec. 5.1. Since these decays increase the particle multiplicity, a slightly smaller value of the a_{SK} would be preferable (see e.g. Figs. 12.3 and 13.1 of Ref. [122]), but the qualitative features would remain the same.

⁶The ISD procedure in Ref. [117] also returns a set of $\{R_{g,i}, z_{g,i}\}$ pairs, but they are in general different from RSD, even for the same β and z_{cut} values, since ISD only follows the trunk of the clustering tree.

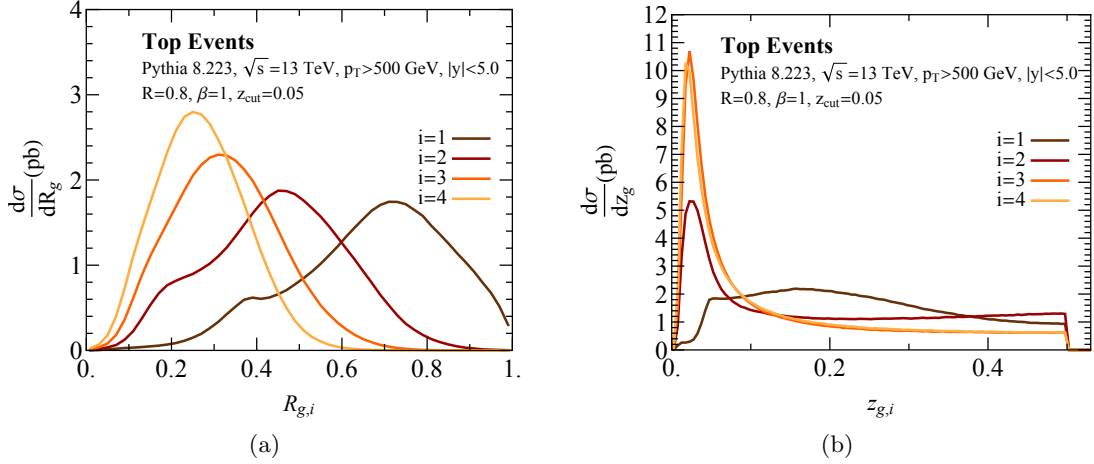


Figure 3. Distributions in the top jet sample of (a) groomed radius and (b) groomed momentum fraction for $i = 1, 2, 3, 4$.

groomed radius of the jet decreases as more layers of RSD are applied. There is a small kink structure at lower values of R_g for $i = \{1, 2\}$ due to the presence of W jets in the top quark decay. In Fig. 3b we show the $z_{g,i}$ distributions, and find that the momentum fraction of the groomed jet is also peaked at values closer to zero as i increases. The sharp cut at 0.5 is because z_g is defined as the relative momentum fraction of the softer subjet, which can be at most half. For $i = 1$, the $z_{g,i}$ distribution has a nontrivial structure from cases where the clustering history differs from the expected $t \rightarrow bW$ topology.

The case of $N = 2$ yields a three-pronged grooming strategy, which may be useful for the study of boosted top decays, and we explore this possibility in Sec. 4.5. Alternatively, one can use the $\{R_{g,i}, z_{g,i}\}$ values directly to discriminate signal events from backgrounds. For example, we can use ratios like $R_{g,3}/R_{g,2}$ as a probe for boosted top jets, somewhat analogous to the use of the N -subjettiness ratio τ_{32} [20, 21]. Similarly, one can use the $z_{g,1}$, and $z_{g,2}$ observables to distinguish QCD-like $1 \rightarrow 2$ parton splittings (see e.g. [104]) from hard $t \rightarrow bW$ and $W \rightarrow q\bar{q}'$ decays. In practice, though, top taggers built from $R_{g,i}$ and $z_{g,i}$ do not seem to perform quite as well as N -subjettiness (with RSD_∞ grooming), but might remain useful inputs for multivariate analyses, depending on how much $R_{g,i}$ and $z_{g,i}$ are correlated with N -subjettiness.

3.2 Non-perturbative effects

Analytical control in jet substructure is mainly limited to perturbative QCD effects. Because internal jet properties probe very exclusive kinematic regions, however, it is not uncommon for non-perturbative effects to yield substantial corrections to perturbative predictions. As such, an important ingredient for robustness of a grooming or tagging algorithm is having a limited sensitivity to non-perturbative contributions, such as hadronization or underlying event. This robustness has already been demonstrated for the mMDT and SD algorithms [28, 42], and we present here a similar analysis for RSD.

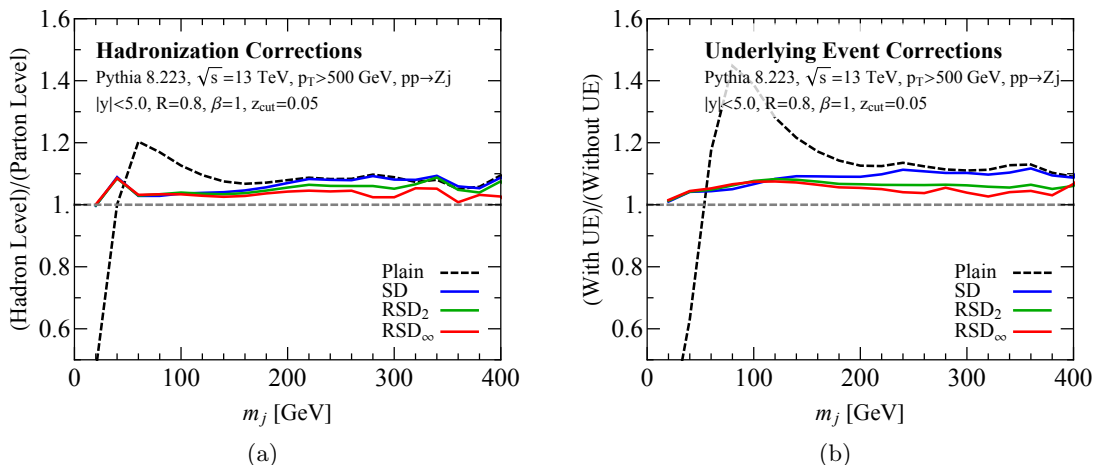


Figure 4. Study of (a) hadronization and (b) underlying event corrections for different N values, with $\beta = 1$ and $z_{\text{cut}} = 0.05$. Shown are ratios of the groomed jet mass spectrum as non-perturbative effects are included in PYTHIA.

We use the process $pp \rightarrow Z + j$ to generate samples of background QCD jets, and use the benchmark RSD parameters $\beta = 1$ and $z_{\text{cut}} = 0.05$. In Fig. 4a, we plot the ratio of the jet mass distributions before and after the hadronization step in PYTHIA. Without any grooming, there are around 10% hadronization corrections throughout the whole distribution, with large corrections below a jet mass of $m_j \sim 50$ GeV. With RSD $_N$, though, the distribution is significantly more stable down to jet masses of around 20 GeV, independent of the number of RSD layers. Remarkably, in the bulk of the distribution between 50–400 GeV, RSD $_{\infty}$ exhibits around 5% hadronization corrections. At large mass, the RSD results also show a sizable improvement as one increases the number of RSD layers.

In Fig. 4b, we show the impact of underlying event, plotting the ratio of the jet mass distributions before and after the inclusion of multiple parton interactions (MPI). Here again, we see a similar behavior for all $N > 0$ curves in the small mass limit, with relatively small corrections due to non-perturbative underlying event effects. We observe furthermore that as $N \rightarrow \infty$, the stability of the jet mass distributions improves substantially at high masses, such that the overall corrections are less than 10% throughout the distribution. It is therefore clear that RSD with $\beta > 0$ substantially improves the robustness of groomed jets to non-perturbative effects, notably by providing more stable results than SD for large jet masses. We also checked that the jet p_t was stable to both hadronization and underlying event effects, with similar performance for all $N \geq 1$.

3.3 The $N \rightarrow \infty$ limit of zero-area jets

An interesting property of RSD groomed jets is that their catchment area [112] goes to zero in the $N \rightarrow \infty$ limit. This is due to the fact that soft ghost particles with infinitesimal energy always fail the SD condition in Eq. (2.1) for $\beta \geq 0$, such that the final jets always

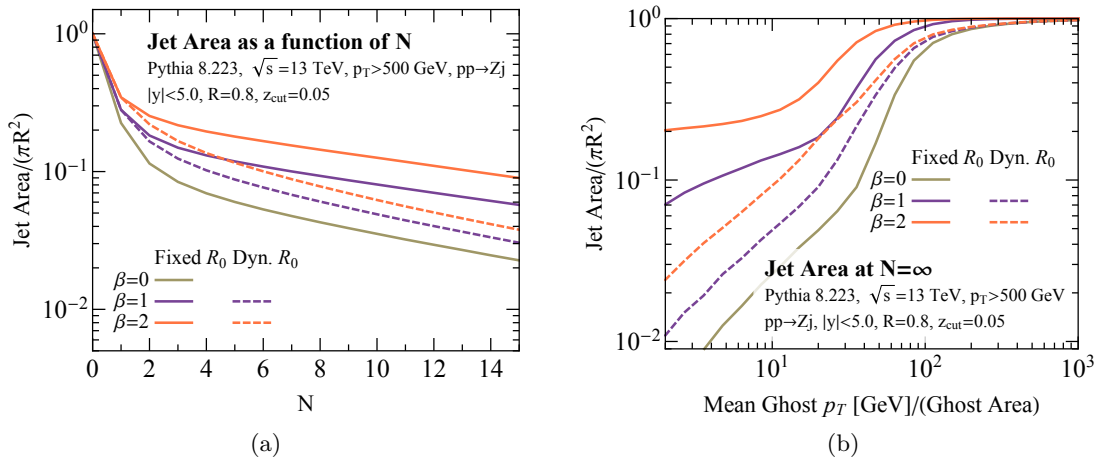


Figure 5. Jet area studies on quark/gluon jets in $pp \rightarrow Zj$ events, for the fixed R_0 (solid line) and dynamic R_0 (dashed line) algorithms. (a) Active jet area as a function of the number of soft drop layers N . (b) Active jet area as a function of ghost transverse momentum density ρ for RSD_∞ .

have vanishing active and passive areas.⁷ For this reason, one might expect that RSD jets would be particularly robust to pileup contamination, a feature we will explore further in Sec. 5. That said, many of the commonly used pileup mitigation techniques, such as the area-median method [112, 114], rely in some way on the jet area. Applying these methods to zero-area jets, obtained when grooming with RSD_∞ , requires some care (see Sec. 5.2).

In Fig. 5a, we use the same $pp \rightarrow Z + j$ samples from Sec. 3.2 and plot the active jet area as a function of the number of RSD layers. Here, we fix $z_{\text{cut}} = 0.05$ and scan the exponent $\beta = \{0, 1, 2\}$, and we explore both the fixed R_0 and dynamic R_0 variant from Sec. 2.3. For all choices of β , the active jet area decreases exponentially with N , as anticipated. For smaller β , the algorithm is more aggressive at removing soft radiation, such that the jet area decreases the most rapidly for $\beta = 0$. In Fig. 5a, one can see that the dynamic R_0 algorithm yields jets with smaller active area for any given β value. In this way, dynamic R_0 behaves more closely to the $\beta = 0$ limit of the fixed R_0 algorithm, leading to decreased pileup sensitivity.

Although RSD_∞ leads to zero-area jets in a formal sense, soft particles from, say, pileup have finite energy in an experimental setting. In Fig. 5b, we plot the effective jet area for RSD_∞ with finite-energy ghost particles, again considering $\beta = \{0, 1, 2\}$. Here, we report the ghost transverse momentum flow density per unit area, which is roughly 0.5 GeV per 1.0×1.0 bin in rapidity/azimuth for one minimum bias collision. For transverse momentum flow densities starting around 50 GeV—below the pileup p_t densities anticipated at the high-luminosity LHC [127]—we observe that while the jet area after RSD_∞ grooming is reduced, it remains substantially above zero even in the $N = \infty$ limit. This behavior explains in part why RSD is not sufficient in itself to remove pileup, and instead performs best when combined with another pileup mitigation technique, as discussed in Sec. 5.

⁷This zero-area feature is also shared by the semi-classical jet algorithm [125] and the “priority” jet algorithm [126]. A key difference is that RSD can be applied to standard anti- k_t jets.

4 Improved mass resolution

The simplest way to identify a boosted hadronically-decaying resonance is through the invariant mass of its decay products; in a contamination-free setting, this would correspond to the plain jet mass. In practice, though, the jet mass is particularly sensitive to unassociated soft wide-angle emissions which smears out the distribution. To restore the mass resolution, it is therefore necessary to mitigate soft contamination through appropriate grooming.

While mMDT and SD are not always the most effective methods for enhancing the signal efficiency for boosted objects, they have the advantage of being particularly robust [48]. As seen in Sec. 3.2, hadronization and underlying event effects are suppressed, and they have an analytically-tractable behavior due to the absence of double logarithms and leading non-global contributions [28, 128, 129]. To maximize the tagging performance, though, Ref. [12] found that MDT grooming should be supplemented by an extra filtering step to improve the jet mass resolution. The hope is that an algorithm like RSD_∞ could, by extending the grooming procedure down to smaller angular scales, achieve excellent mass resolution without requiring any further post-processing.

In this section, we study the mass resolution with RSD in three cases of interest for the LHC: 2-prong boosted W bosons, 3-prong boosted top quarks, and 4-prong boosted Higgs jets ($H \rightarrow VV \rightarrow 4f$). In each case, we use the same PYTHIA 8.223 generator settings from Sec. 3, and consider all jets in the event that pass the selection cuts $p_t > 500$ GeV and $|y| < 5$. As we will see, RSD provides a way to improve the achievable resolution, with gains in the 10-20% range, while retaining the tractability and robustness of SD.

Our overall recommendation from these studies will be to use RSD_∞ with the default settings of $\beta = 1$ and $z_{\text{cut}} = 0.05$, which gives good performance across the three test cases. (although other values of β and z_{cut} are worth investigating as well). This conclusion will persist even after the inclusion of pileup in Sec. 5.1, making RSD_∞ useful in extreme environments such as the one faced by the high-luminosity LHC.

4.1 Definition of the mass peak and resolution

To define the mass resolution, we identify the *smallest* mass interval that contains a fixed fraction f of the total event samples (see e.g. [3]). For concreteness, we set $f = 0.4$ for these studies. The central value is then defined as the median of the mass interval, and the width is defined as the width of the mass interval.

An alternative approach would be to fit the mass distribution with two curves, a narrow Cauchy distribution to capture the signal and a wider background distribution to account for cases of poor reconstruction. The advantage of the interval method is that it allows us to avoid biases associated with the choice of a fitting functional form. That said, we did test the fitting approach and got similar qualitative features to the ones shown here. We also tested that the choice of fraction f did not affect the qualitative conclusions.

One caveat of the interval method is that it combines two logically distinct effects: mass resolution and signal efficiency. For example, if a technique yields perfect mass resolution, but only on a small subsample of events, then the mass interval will be larger than the

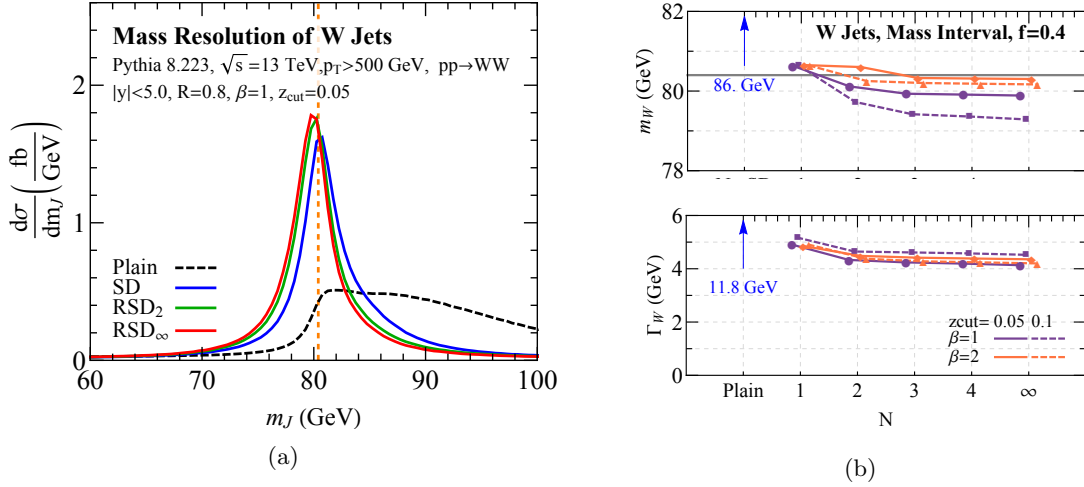


Figure 6. (a) Mass distributions for the W jet sample using different levels of RSD and the benchmark values of $\beta = 1$ and $z_{\text{cut}} = 0.05$. (b) Central mass values and widths as a function of N , testing four different β and z_{cut} combinations, using a mass interval containing a fraction $f = 0.4$ of the events.

resolution in order to include the fixed fraction f . In practice, though, many boosted-object taggers select jets based on a fixed mass window, so our definition of mass resolution is appropriate for that setting.

4.2 Two-prong W decays

In Fig. 6a, we show the jet mass distribution from a W jet sample obtained from $pp \rightarrow WW$, with the W decaying hadronically. At least some level of grooming is required to obtain a peak within 10% of the W mass. With $\beta = 1$ and $z_{\text{cut}} = 0.05$, the jet mass distribution is already close to the expected W mass value after applying SD alone. Adding additional SD layers with $N \geq 2$, the peak shifts somewhat below the expected W mass value, but, more importantly, the width of the mass distribution decreases. Another interesting observation is that the mass distribution is more symmetric with additional grooming layers, such that with $N = \infty$, the jet mass can be accurately fit by a Cauchy distribution.

To get a sense of the dependence on the choice of RSD parameters, in Fig. 6b we plot the central value and width of the mass distribution as a function of N . As discussed in Sec. 4.1, we use a mass interval containing a fraction $f = 0.4$ of events. The benchmark parameters of $\beta = 1$ and $z_{\text{cut}} = 0.05$ undershoot the W mass central value by around 1 GeV, while switching to $\beta = 2$ gives a better reconstruction of the central value. On the other hand, the benchmark parameters yield the best W mass resolution, which implies somewhat better tagging performance. More generally, all of the RSD settings yield a sizable improvement over the ungroomed case and a smaller but clearly visible improvement, of order 10–20%, over the SD case in terms of resolution.

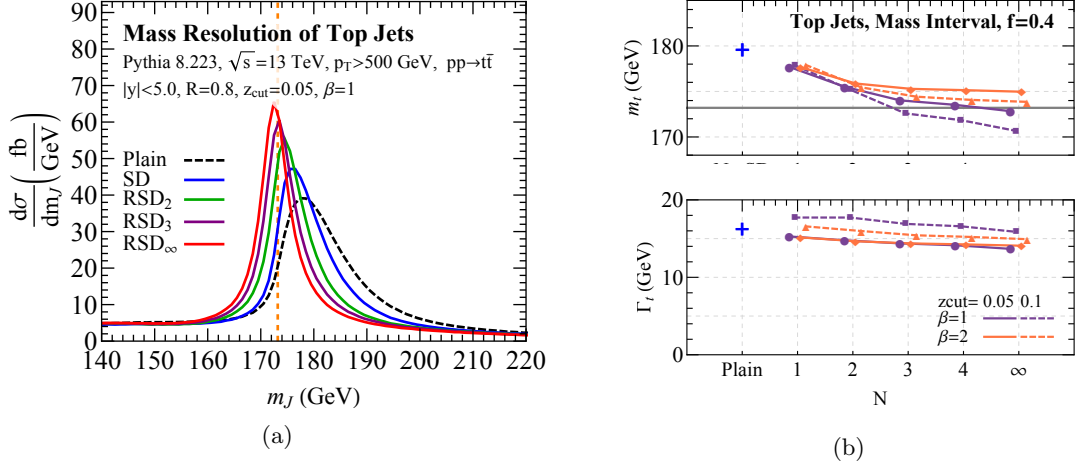


Figure 7. Same as Fig. 6 but for the top jet sample.

4.3 Three-prong top decays

Unlike SD, which terminates after probing only the leading two subjets, RSD with $N > 1$ is well suited to handle the broad radiation patterns and three-prong topologies of top quarks. We consider a sample of $pp \rightarrow t\bar{t}$ events, where the top mass in PYTHIA is set to 173.2 GeV. In Fig. 7a, we show the mass distribution of boosted tops for different layers of RSD. As expected, we find that without grooming, the peak of the distribution occurs at values well above the top mass. With successive layers of RSD grooming, the mass peak shifts to lower values, and converges very close to the top mass for $N = \infty$. This is due to the fact that we discard more of the extra unassociated radiation, and therefore the mass tends to decrease.

In Fig. 7b, we consider the central mass value and width containing a fraction $f = 0.4$ of the mass distribution. We find that $\beta = 1$ and $z_{\text{cut}} = 0.05$ gives nearly optimal performance (by the mass interval measure), with $\beta = 2$ and $z_{\text{cut}} = 0.1$ giving comparable performance in terms of accuracy and resolution. The gain in resolution compared to SD is found to be slightly larger than 10%.

Compared to the W case in Sec. 4.2, where the resolution tends to saturate by $N = 2$, the top case benefits from taking $N \geq 3$. In fact, there is a marginal benefit from taking $N \rightarrow \infty$, which is why we recommend RSD_∞ for mass resolution studies involving the top quark. It would be interesting to see whether RSD_∞ would also be appropriate for defining a short-distance top quark mass [130].

4.4 Four-prong Higgs decays in associated production

Four-prong jets can provide important information in certain Higgs decays, where the $H \rightarrow VV \rightarrow 4f$ channel plays an important role in determining properties of the Higgs [131] as well as its couplings to bosons [132]. They can also provide a useful probe for new physics, such as in hadronic decays of heavy resonances decaying to HW or HZ [81], or in hadronic decays of a boosted Higgs pair [133].

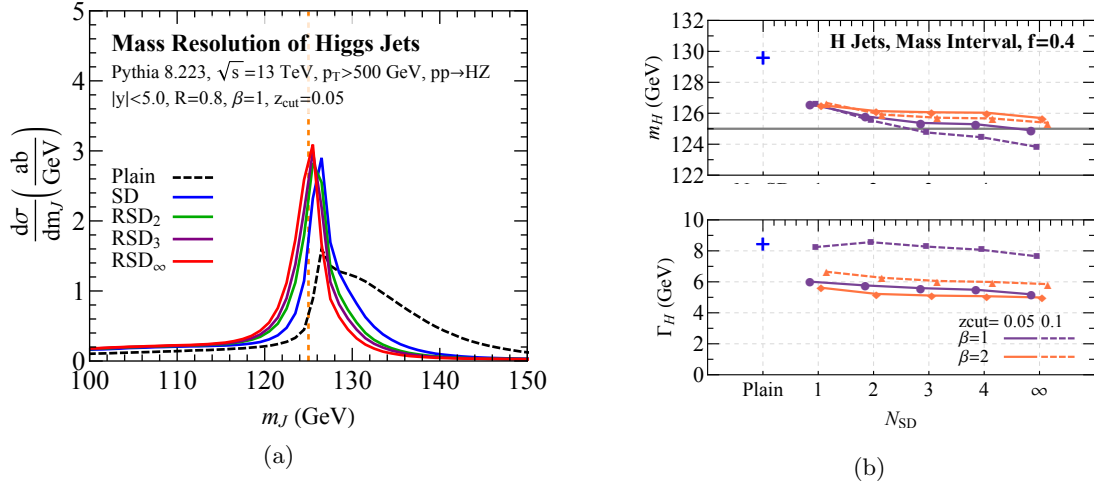


Figure 8. Same as Fig. 6 but for the Higgs jet sample.

In Fig. 8a, we show the reconstructed Higgs mass in boosted $H \rightarrow W^+W^- \rightarrow q\bar{q}q\bar{q}$ decays. This comes from a sample of $pp \rightarrow HZ$ events, with the Z boson decaying to neutrinos. Although grooming with ordinary SD performs relatively well, the Higgs mass reconstruction is better with $N \geq 3$, as one would expect for a four-particle decay. A comparison of the central mass values and width for different grooming parameters is shown in Fig. 8b, showing gains in resolution around 10–15%. Once again, the benchmark choice of $\beta = 1$ and $z_{\text{cut}} = 0.05$ gives an excellent reconstruction, especially in the $N \rightarrow \infty$ limit, although $\beta = 2$ and $z_{\text{cut}} = 0.05$ gives a slightly better resolution.

4.5 Boosted top tagging

We conclude this section with a concrete example of the impact of improved mass resolution from RSD. Using the same samples as Sec. 4.3, we perform a study of boosted top tagging performance. We consider two standard observables used for discriminating top jets from QCD background: the N -subjettiness ratio $\tau_{32} = \tau_3/\tau_2$ [20, 21], and the generalized energy correlation function ratio $N_3^{(2)} = 2e_4^{(2)}/(e_3^{(2)})^2$ [22, 25]. By adjusting the degree of grooming—on both the jet mass and on the jet discriminant—we can assess the potential performance gains from RSD.

In Fig. 9, we plot the top signal efficiency versus dijet background mistag rate (ROC curves). The rightmost endpoints of the ROC curve indicate the impact of an overall cut of $m_{\text{groomed}} \in [160, 185]$. As N increases, the dijet mistag rate improves somewhat, and the top signal efficiency increases due to the improved mass resolution. The rest of the ROC curve is associated with sweeping a cut on τ_{32} and N_3 . Note that as the substructure cut becomes more stringent, there is less of a gain from increasing the number of grooming layers. The reason is that grooming removes part of the radiation phase-space where there is still some discriminating power, or equivalently, a cut on τ_{32} or N_3 already removes some of the phase-space regions targeted by grooming. Because this phase-space region is also the most sensitive to non-perturbative effects, there is a tradeoff between tagging

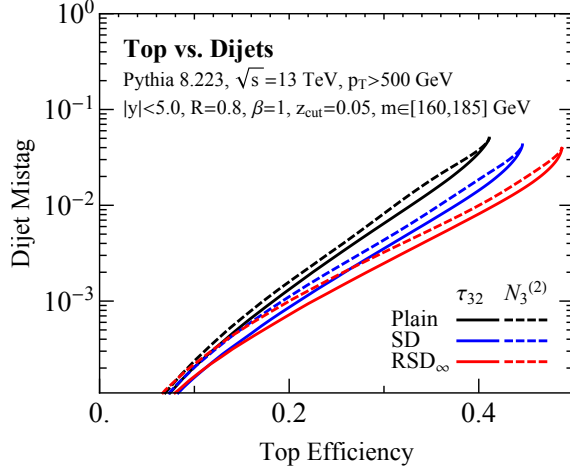


Figure 9. Top jet signal efficiency versus dijet background mistag rate, with the benchmark RSD parameters of $\beta = 1$ and $z_{\text{cut}} = 0.05$.

performance and non-perturbative robustness [48]. Despite this tradeoff, RSD_∞ maintains the best tagging performance for top efficiencies greater than 10%.

As discussed in Ref. [25], τ_{32} with grooming and N_3 with grooming have the same soft-collinear power counting, so their performance is expected to be similar (see further discussion in Ref. [24]). This conclusion persists even with multiple grooming layers. The relative difference between τ_{32} and N_3 then depends on the precise details of the event selection. N_3 is not defined with respect to any axes, so it is expected to perform better than τ_{32} in kinematic regimes where the choice of axes can be ambiguous [25]. Here, though, we are taking a rather tight mass window of $m_{\text{jet}} \in [160, 185]$ GeV, so the axes effects are subleading and τ_{32} turns out to give better performance. Though not shown, we also tested the performance of the M_3 observable [25]. While M_3 always performs worse than τ_{32} or N_3 , the relative improvement in going from SD to RSD_∞ is greater due to the removal of radiation in all three prongs.

We found similar tagging results for other boosted objects, such as hadronic decays of boosted W and Higgs bosons. In general, RSD_∞ gives similar or improved performance compared to tagging with SD, though most of that comes just from the improved mass resolution. For the case of W tagging, it would be interesting to study a version of the dichroic N -subjettiness ratio [49], where RSD_∞ is used to compute the jet mass and τ_1 (or $1e_2$), and a lighter grooming, like (R)SD with larger β and smaller z_{cut} , is used to calculate τ_2 (or $2e_3$). Results for boosted top tagging with large pileup multiplicity are shown in App. B.2.

5 Robust pileup mitigation

As the LHC progresses towards ever higher luminosities, mitigating the effect of secondary proton-proton collisions becomes an increasingly important challenge. Large pileup levels can substantially impact typical jet observables, increasing for example the jet’s mo-

mentum, while shifting and distorting jet shapes. A number of techniques have been developed to remove soft radiation associated with secondary vertices. These include area–median [112, 114] or shape [134] subtraction; grooming with trimming [15], pruning [17], or mMDT/SD [28, 42]; charged hadron subtraction [135]; particle-level removal methods such as SoftKiller [113] and PUPPI [136]; and machine learning methods [137]. In practice, in the context of jet substructure, it is generally most useful to combine a removal or subtraction method with some type of jet grooming to achieve optimal results (see e.g. [3]).

Here, we investigate the properties of jets after grooming with RSD under varying levels of pileup, with additional pileup studies appearing in App. B. We will see that, when used in combination with SoftKiller [113], the RSD algorithm yields robust pileup mitigation results even under high pileup conditions.⁸ We will also test RSD with the area–median subtraction approach [114].

5.1 Mass resolution with SoftKiller

SoftKiller is an event-wide particle-level removal method, which uses a dynamic cut on transverse momentum p_t^{cut} to remove soft particles [113]. The threshold is determined dynamically on an event-by-event basis as follows:

1. The event is split into patches of size $a_{\text{SK}} \times a_{\text{SK}}$ in rapidity–azimuth space.
2. For each patch, one determines $p_{t,i}^{\text{max}}$, the largest particle transverse momentum in patch i .
3. The transverse momentum threshold p_t^{cut} is determined by

$$p_t^{\text{cut}} = \text{median}_i (p_{t,i}^{\text{max}}) , \quad (5.1)$$

where the median is taken across all patches.

4. All particles with transverse momenta below p_t^{cut} are removed from the event.

An equivalent description of SoftKiller is finding the minimal p_t^{cut} such that exactly half of the patches have zero momenta. This p_t^{cut} ensures that the median across patches of transverse-momentum flow per unit area ρ is zero.⁹

For each analysis, one has to set the appropriate patch size by choosing the SoftKiller parameter a_{SK} . The goal is to set the parameter a_{SK} to minimize both the shift in jet p_t and mass. After RSD grooming of $R = 0.8$ jets, this is usually achieved with $a_{\text{SK}} = 0.5$, although this was found to be somewhat process dependent.¹⁰ For the case of $pp \rightarrow t\bar{t}$, the dependence of the jet mass on the choice of grid parameter is shown in Fig. 10. We find that the position of the top peak depends significantly on the value of a_{SK} with small (large)

⁸Applying RSD without any pileup mitigation shows poor performance, so we have not included those results in our discussion.

⁹The quantity ρ is computed via $\rho = \text{median}_i \left(\frac{p_{t,i}}{A_i} \right)$, where A_i is the patch area and $p_{t,i}$ is the transverse momentum of the patch.

¹⁰The optimal choice of a_{SK} would also change if we were to include π^0 and B -hadron decays in our simulation or if we were performing charge-hadron subtraction or including a calorimeter simulation [113].

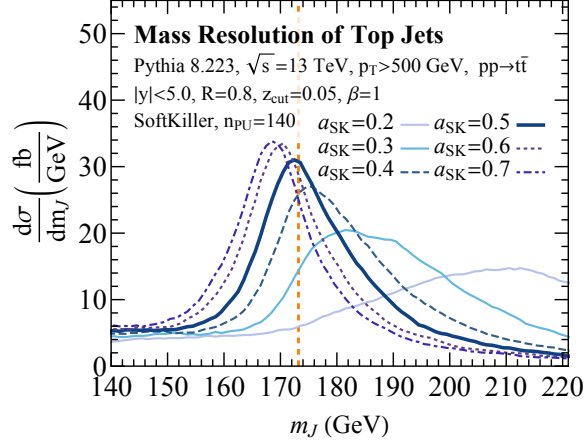


Figure 10. The RSD groomed mass distribution for multiple values of the SK grid parameter a_{SK} .

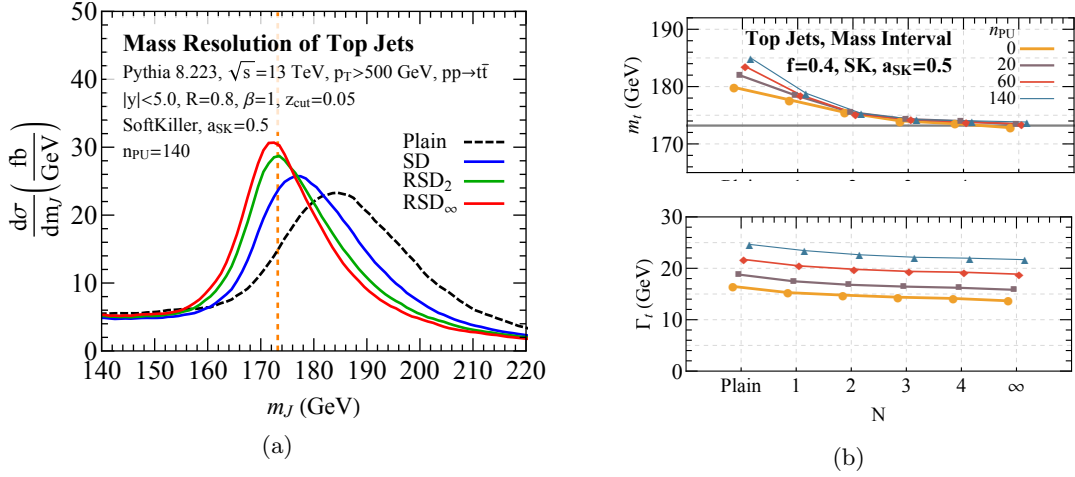


Figure 11. (a) Same as Fig. 7a, but with 140 pileup vertices and using a SoftKiller parameter of $a_{SK} = 0.5$. (b) Central mass values and widths as a function of N for several pileup multiplicities, using the benchmark RSD/SoftKiller parameters and $f = 0.4$.

values of a_{SK} showing a clear undersubtraction (oversubtraction). In our simulations, $a_{SK} \simeq 0.5$ shows only a small average bias, so we take this value as our benchmark.

We now study the effects of pileup on the mass resolution in groomed jets, following the same analysis strategy as Sec. 4. Since the behavior is quite similar to that observed previously, we focus here only on top events, with the W and Higgs cases discussed in App. B.1.

We use the same $pp \rightarrow t\bar{t}$ process as in Sec. 4.3, with the PYTHIA top mass at 173.2 GeV. In Fig. 11a, we show the top jet mass distribution with the addition of 140 pileup vertices. With SoftKiller but without any jet grooming, there is a 12 GeV shift in the reconstructed top mass peak. (The shift would be larger than 200 GeV if SoftKiller were not applied.) The shift decreases to about 5 GeV after applying SD, with additional improvements in going to RSD_2 and RSD_∞ . Though the shape of the top mass distribution is not nearly as

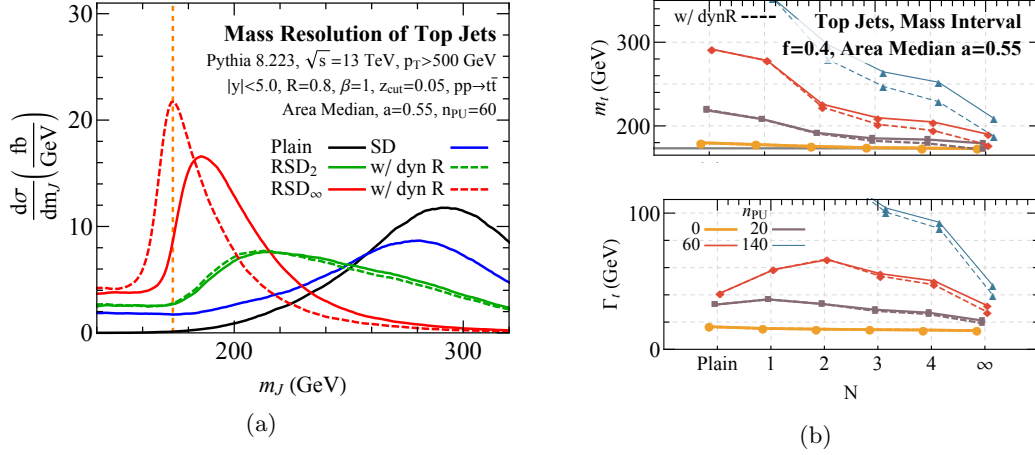


Figure 12. (a) Similar to Fig. 11a, but with 60 pileup vertices and using an area–median parameter of $a = 0.55$. Note the larger mass range shown and the inclusion of both fixed- R_0 and dynamic- R_0 results. (b) Same as Fig. 11b but for the area–median method applied to RSD with dynamic R_0 .

symmetric as without pileup, RSD_∞ does restore some of the symmetry of the top mass distribution compared to SoftKiller alone.¹¹

In Fig. 11b, we show the central mass value and width after the application of SoftKiller and RSD_N for several pileup levels. As n_{PU} increases from 0 to 140, the central top mass value and the width increases monotonically, even with the application of SoftKiller. By applying more layers of RSD, the central top mass decreases toward the physical value, with somewhat improved stability across the different pileup levels. The best performance is obtained for RSD_∞, in agreement with the analysis of Sec. 4.3, and the mass difference is less than 5 GeV even at the highest pileup level. This shows that, as well as improving the resolution of observables such as the jet mass, grooming with RSD somewhat improves the stability of the distributions as a function of the number of pileup vertices n_{PU} . That said, there are still substantial distortions to the width of the top mass distribution even after RSD_∞, reflecting the underlying challenge of pileup at the LHC.

5.2 Mass resolution with the area–median method

Let us now consider pileup mitigation using RSD in conjunction with the area–median method [112, 114]. This removal technique is widely used in experimental analyses, and we therefore provide a short study of its use with RSD groomed jets.

Generally speaking, combining the area–median procedure with grooming requires more than just subtracting the jet after grooming. Indeed, since the grooming procedure imposes kinematic constraints on subjets, one wants to apply the subtraction procedure directly on the subjets, so that these kinematic constraints use quantities which have been

¹¹As shown in Ref. [113], one can get better performance for SoftKiller alone by increasing the grid-size parameter a_{SK} . Even if this works for correcting for the mass shift, however, it results in much broader peaks than what we obtain here by combining SoftKiller with (R)SD.

corrected for pileup (see e.g. [3]). In the case of RSD (and mMDT/SD), this means that, at each step of the declustering procedure, we should apply an area–median subtraction to both subjects before imposing the SD condition in Eq. (2.1).¹² Note that even in the case of RSD_∞ where the final groomed jet has zero area, intermediate subjects have a non-zero area, so subtracting the intermediate subjects is crucial.

The resulting mass peak is shown in Fig. 12a, for both a dynamic and fixed R_0 implementation of RSD for 60 pileup events, using the area–median parameter $a = 0.55$. We find that only the most aggressive algorithm RSD_∞ , preferably using dynamic R_0 from Sec. 2.3, succeeds at reconstructing the top peak. This is confirmed by Fig. 12b, where we show the central mass values and widths for various pileup levels. Despite the fact that RSD_∞ with dynamic R_0 does recover the top mass peak, one should still note that the mass resolution (and median peak position) significantly worsens with increasing pileup multiplicity, encouraging the investigation of more recent particle-level pileup mitigation techniques for future runs of the LHC.

6 Bottom-Up Soft Drop for event-wide grooming

We have seen that the default RSD algorithm in Sec. 2.2 yields sensible grooming behaviors across a wide range of applications, with excellent overall performance for $N = \infty$. It is possible, however, to obtain similar results with a different approach. In this section, we introduce an alternative to RSD_∞ called Bottom-Up Soft Drop (BUSD), which is also available in `RecursiveTools` ($\geq 2.0.0$) through `fastjet-contrib` [118].

The default RSD is a top-down algorithm, where the SD condition in Eq. (2.1) is imposed by declustering a jet starting from its clustering tree. By contrast, BUSD imposes Eq. (2.1) as part of a (re)clustering procedure, effectively starting from the leaves of the clustering tree. BUSD can either be applied to a single jet (*local BUSD*) or to the event as a whole (*global BUSD*).

With either BUSD approach, the SD criteria is applied at each pairwise combination during the reclustering stage, somewhat like pruning [17]. In the `fastjet-contrib` implementation, this is achieved through a modified recombination scheme, such that at each step of the reclustering with a large- R C/A algorithm, the pseudojet obtained from combining particles i and j with smallest distance $d_{ij} = \Delta R_{ij}/R_0$ is given by

$$p_{ij} = \begin{cases} \max(p_i, p_j) & \text{if Eq. (2.1) fails,} \\ p_i + p_j & \text{otherwise,} \end{cases} \quad (6.1)$$

where the maximum is defined by p_t . In the definition of d_{ij} , we choose R_0 to match the SD criteria in Eq. (2.1). For the studies below, we always match the parameter R_0 to the jet radius R .

With local BUSD, the reclustering is applied to an individual jet found by another jet algorithm. While one cannot obtain finite N results with BUSD, the bottom-up algorithm

¹²A similar philosophy is also recommended, but sadly not always implemented, when using other grooming techniques like pruning and trimming.

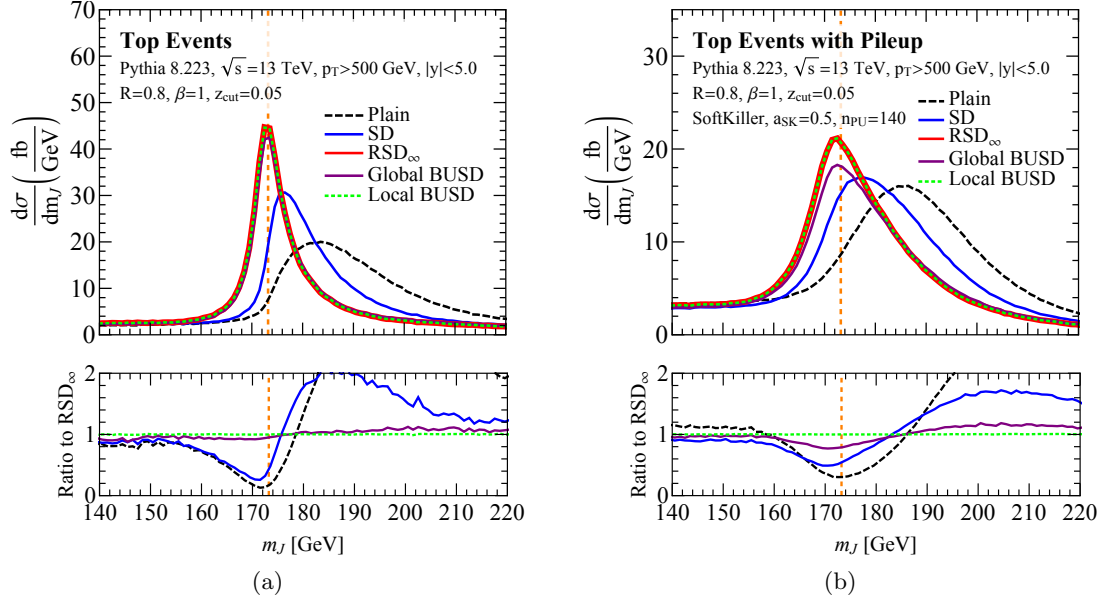


Figure 13. Behavior of global and local BUSD on $t\bar{t}$ events with the default RSD parameters. (a) Performance without pileup, to be compared to Fig. 7a. (b) Performance with 140 pileup vertices plus SoftKiller, to be compared to Fig. 11a. In both panels, the ratios to RSD_∞ are shown at the bottom.

provides results that are very similar to the $N = \infty$ top-down approach of RSD_∞ . This is expected, since local BUSD uses the same initial jet constituents as RSD_∞ .

With global BUSD, the full event is clustered into a single large C/A tree. This provides an event-wide grooming strategy that does not require any specific jet definition. After grooming with global BUSD, the groomed event contains only a subset of the initial particles, so any jet definition can be used to cluster the remaining particles. The resulting jets are guaranteed to have zero active area, without any additional treatment required for each individual jet.

The behavior of BUSD is shown in Fig. 13a for the same $pp \rightarrow t\bar{t}$ sample from Sec. 4.3. Without pileup, RSD_∞ , local BUSD, and global BUSD give nearly identical results on the top jet mass distribution. This suggests that globally grooming an event before the jet clustering stage could be a practical alternative to standard jet-based grooming.

We test the robustness of BUSD to pileup in Fig. 13b. As in Sec. 5.1, we overlay 140 pileup vertices and apply the SoftKiller algorithm with grid parameter $a_{\text{SK}} = 0.5$. There is still nearly identical behavior for RSD_∞ and local BUSD, with somewhat degraded performance seen using global BUSD. So while global BUSD grooming still performs better than the original SD in reconstructing the top mass, it is outperformed by RSD_∞ (and local BUSD) in extreme environments.

7 Conclusions

Recursive Soft Drop (RSD) is a generalization of the original mMDT/SD algorithm, which has already seen successful applications at the LHC. By recursively applying the SD declustering procedure N times, RSD_N can remove jet contamination more efficiently and with looser SD parameters than original SD. With benchmark parameters $\beta = 1$ and $z_{\text{cut}} = 0.05$, we found that RSD grooming performs particularly well in the fully-recursive $N = \infty$ limit. This limit also shows an improved robustness against pileup effects, a feature which is likely connected to the fact that RSD_∞ yields groomed jets with formally zero area.

Jet grooming with RSD provides several refinements over previous techniques, notably by increasing the robustness to non-perturbative effects and by improving the mass resolution for boosted heavy resonances such as W bosons, top quarks, and Higgs bosons. In the context of jet tagging, the additional declustering layers have a modest impact on QCD backgrounds, so much of the gains in tagging performance come from the improved jet mass resolution. While RSD_{N-1} seems to be the natural choice for grooming N -prong objects, we have noticed that adding more grooming layers, e.g. using RSD_N , comes with further resolution gains. In the end, we recommend the use of RSD_∞ , since it offers the same or better performance in our case studies with no discernible downsides. The one possible exception is for boosted W bosons, where RSD_∞ gave a better W boson resolution compared to SD but at the expense of shifting the W peak location by $\mathcal{O}(1)$ GeV. That said, this shift could be minimized by using lower values of z_{cut} or higher values of β .

For pileup mitigation, RSD works best when paired with a particle-level removal algorithm such as SoftKiller. In the presence of pileup, we found substantial improvements in the groomed mass resolution after grooming with RSD when compared to the original SD procedure. We recommend the use of RSD_∞ in high luminosity environments, since this always performed better than RSD with finite N . It is also possible to use RSD with area-based pileup subtraction methods, as long as the corrections are applied on the finite-area subjects that enter into the SD condition.

An interesting alternative to RSD_∞ is Bottom-Up Soft Drop (BUSD). In its local variant, i.e. applied to a single jet, it shows similar performance to RSD_∞ , with comparable resilience to pileup effects. BUSD also admits a global implementation, where it is applied at the event-wide level to groom an event without committing to a particular jet algorithm. This latter variant shows, however, a slightly larger sensitivity to pileup than RSD_∞ .

Since RSD is closely related to the mMDT/SD algorithms, it shares the advantage of retaining analytic tractability. We look forward to future studies aimed at high-precision and systematically-improvable analytical results of tagging rates. These could be achieved with existing frameworks to leading-logarithmic accuracy, and could potentially be extended to higher logarithmic accuracy through a suitable extension of the CAESAR [138] and ARES [139, 140] methods or through a modified factorization theorem [50] in soft-collinear effective theory [141–144]. An interesting potential application of RSD is in defining the short-distance top quark mass using light grooming [130].

Finally, RSD could also find useful applications in the context of heavy ion collisions, where jet grooming can provide a powerful probe into the effects of the medium on the

momentum sharing z_g [106, 109–111]. By adjusting the number of grooming layers N , one can achieve a more aggressive grooming while retaining more of the underlying hard scattering process. Furthermore, the groomed energy fractions $z_{g,i}$ obtained at every SD layer i may provide an additional handle to study the propagation of partons through the quark-gluon plasma at multiple resolution scales.

Acknowledgements

We would like to thank Yang-Ting Chien, Andrew Larkoski, and Ian Mould for useful discussions, as well as Mrinal Dasgupta and Simone Marzani for comments on the manuscript. FD is supported by the SNF grant P2SKP2_165039. FD and JT are supported by the Office of High Energy Physics of the U.S. Department of Energy (DOE) under grant DE-SC-0012567. GS’s work is supported in part by the French Agence Nationale de la Recherche, under grant ANR-15-CE31-0016. LN’s work is supported by the DOE under Award Number DE-SC-0011632, and the Sherman Fairchild fellowship.

A Behavior at fixed order

In this appendix, we study the behavior of RSD at fixed order in α_s . To this end, we use **Event2** [145, 146] to produce a sample of boosted heavy bosons decaying (at tree level) to a quark-antiquark pair. We start from an e^+e^- collision at a given center-of-mass energy $M \equiv \sqrt{s}$, corresponding to the mass of the heavy boson. Then, we boost the partonic system transversely such that the heavy boson is traveling along the x axis of the collision with transverse momentum p_t . In what follows, we fix $M = 100$ GeV and $p_t = 500$ GeV. We cluster the event with the anti- k_t algorithm with $R = 0.8$, and we apply RSD_N with $\beta = 1$, $z_{\text{cut}} = 0.2$, varying the number of layers N . Note the use of a larger z_{cut} value compared to our recommended default to make the impact of RSD more visible.

The motivation for studying such boosted systems is that it provides a source of jets with 2, 3, and 4 partons at respective orders α_s^0 , α_s^1 , and α_s^2 , allowing us to study the effects of several layers of RSD.

Let us start by discussing the jet mass in Fig. 14a. Instead of plotting the mass distribution after applying RSD_N , we plot the difference

$$\Delta\sigma_N(m) = \frac{1}{\sigma_{\text{Born}}} \left[\left. \frac{d\sigma}{dm} \right|_{\text{RSD}_{N+1}} - \left. \frac{d\sigma}{dm} \right|_{\text{RSD}_N} \right], \quad (\text{A.1})$$

i.e. the difference in the mass spectrum between two consecutive layers of RSD. From top to bottom, Fig. 14a shows $\Delta\sigma_N$ for tree-level events ($e^+e^- \rightarrow q\bar{q}$) at $\mathcal{O}(\alpha_s^0)$, the order α_s correction, and the order α_s^2 correction.

At $\mathcal{O}(\alpha_s^0)$, there is either one or two partons in the jet. For one parton, the jet mass is always zero, irrespectively of the number of layers of RSD. Jets with two partons, however, have a (plain) jet mass M . Therefore, if we apply $\text{SD} = \text{RSD}_1$ to such a jet, we can either have a jet with two partons and a mass M , or a jet with one parton and a zero mass, depending on whether or not the SD condition is satisfied. Since there is no additional

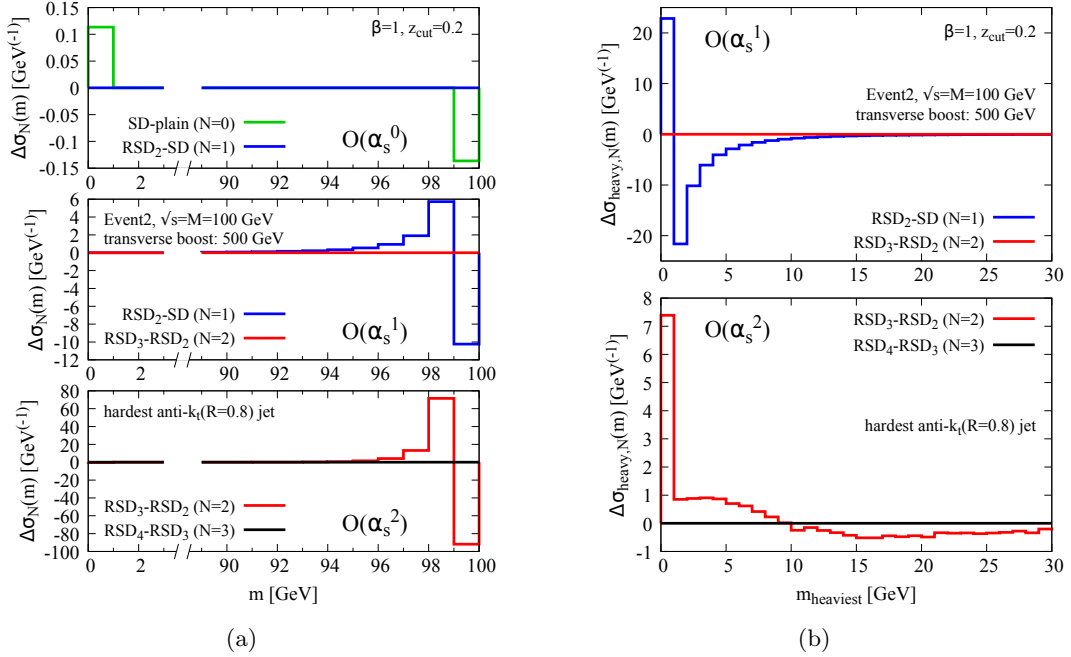


Figure 14. Fixed-order coefficients from Event2 for (a) the jet mass distribution and (b) the heavier subjet mass distribution. The plot shows Eq. (A.1), the difference in the jet mass spectrum obtained with consecutive layers of RSD.

substructure to probe in the jet, applying additional SD layers with $\text{RSD}_{N>1}$ will not have any effect. This expectation is indeed observed in the top panel of Fig. 14a: applying the first layer of SD yields a decrease of the cross section for $m = M = 100$ GeV and an increase at zero mass, i.e. $\Delta\sigma_0 \neq 0$, and additional SD layers have no effect, i.e. $\Delta\sigma_{(\geq)1} = 0$.

At order α_s , we now have jets with three partons, which is enough to see a non-trivial effect from RSD₂. Indeed, if we have a jet with three partons for which the first declustering passes the SD condition, the second SD layer will sometimes be applied on a subjet itself made of two partons; if this system fails the SD condition, the RSD₂ mass will be smaller than the RSD₁ mass, with all subsequent layers being ineffective. This is seen in the middle panel of Fig. 14a, with $\Delta\sigma_1$ showing a shift towards smaller masses and $\Delta\sigma_{(\geq)2} = 0$.

Unsurprisingly, the same pattern is observed at order α_s^2 , just one layer further down, with $\Delta\sigma_2$ showing a decrease in mass while $\Delta\sigma_{\geq 3} = 0$. Note that although the two-loop virtual corrections, contributing at $O(\alpha_s^2)$, are not available in Event2, they correspond to events where the jets can have at most two partons and so do not contribute to $\Delta\sigma_{N\geq 1}$. Ultimately, we see that each successive SD layer further grooms the jet. For the N^{th} layer of SD to be effective, one needs at least $N+1$ partons in the jet, hence $\Delta\sigma_N$ being non-zero starting at order α_s^N .

In addition to the jet mass distribution, we can also study the mass spectrum of the heavier subjet in a jet, shown in Fig. 14b. This is defined by applying RSD to the jet and taking, in the resulting groomed jet, the heavier of the two subjets corresponding to the *first* declustering that has passed the SD condition. Taking the example of Fig. 2, this is

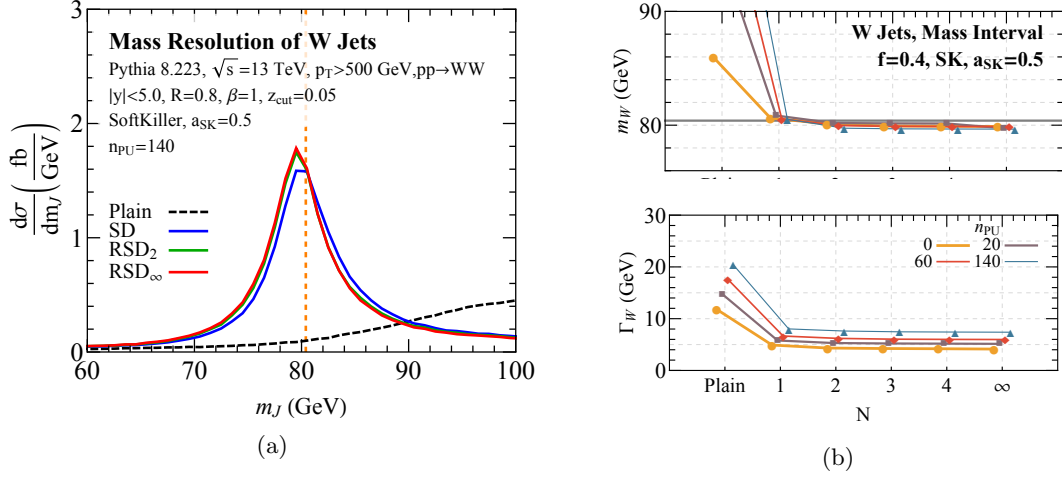


Figure 15. Same as Fig. 11 but for the W boson sample.

the heavier of the RSD subjects tagged at vertex “1”, i.e. the heavier of the subject made of the two upper kept particles and the subject made of the two lower kept particles.

At $\mathcal{O}(\alpha_s^0)$, there can be at most one particle in a subject so the heavier subject mass is always 0. At higher orders, though, one can get more partons and hence a non-zero subject mass. We study the difference $\Delta\sigma_{\text{heavy},N}(m)$ in Fig. 14b, defined analogously to Eq. (A.1) as the difference in the heavier subject mass distribution between N and $N+1$ layers of RSD. As with the jet mass, we need at least $N+2$ partons in the jet to get a non-zero $\Delta\sigma_{\text{heavy},N}$, a situation which starts at order α_s^N . This is confirmed by our **Event2** simulations where, for example, $\Delta\sigma_{\text{heavy},1}$ is already different from zero at $\mathcal{O}(\alpha_s)$ while $\Delta\sigma_{\text{heavy},2}$ starts being non-zero at $\mathcal{O}(\alpha_s^2)$.

A calculation of the logarithmically-enhanced terms appearing in these distributions could serve as a base for an analytic study of RSD.

B Additional pileup studies

In this appendix, we present additional results for RSD in high pileup conditions.

B.1 W and Higgs mass resolution with SoftKiller

Analogously to the case of 3-pronged top decays in Sec. 5.1, here we show results for 2-prong boosted W bosons and 4-prong boosted H bosons. In all cases, we use the default RSD parameters $\beta = 1$ and $z_{\text{cut}} = 0.05$, and apply SoftKiller with $a_{\text{SK}} = 0.5$.

The W mass distribution is shown in Fig. 15a, with the addition of 140 pileup vertices. This is using the same event samples as in Sec. 4.2 and can be compared to Fig. 7a. Already, the performance is very good for SD alone, though the mass resolution is improved somewhat going to RSD₂ or RSD_∞. Note that the distribution becomes a bit more symmetric, though not nearly as much as in the case without pileup. In Fig. 15b, we show the central mass value and width as a function of number of SD layers for different pileup

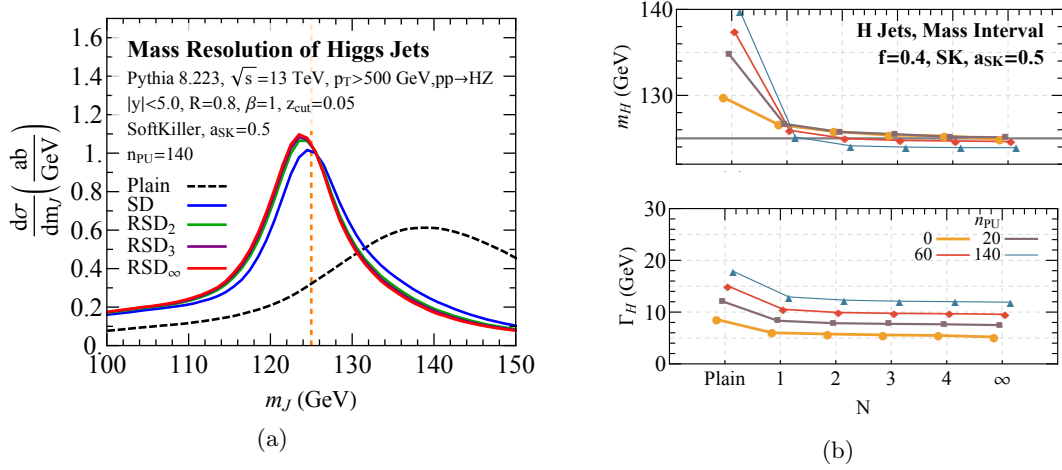


Figure 16. Same as Fig. 11 but for the $H(\rightarrow 4q)$ boson sample.

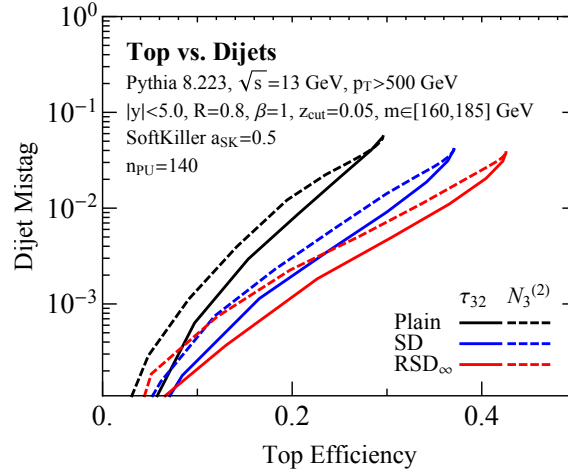


Figure 17. Same as Fig. 9, but with 140 pileup vertices and SoftKiller with grid parameter $a_{\text{SK}} = 0.5$.

levels. One can see that as N increases, the peak location improves while the distribution becomes narrower, though the performance basically saturates at $N = 2$.

In Fig. 16a we show the mass distribution for $H \rightarrow 4q$ decays, again with 140 pileup vertices. This is using the same event samples as in Sec. 4.4 and can be compared to Fig. 8a. Again, one can observe a small improvement in both the location of the central value and the width of the distribution as the number of SD layers is increased. This is shown more explicitly in Fig. 16b, where we can see the narrowing of the distribution and convergence of the peak for different pileup levels, with performance saturating around $N = 3$ or $N = 4$.

B.2 Boosted top tagging with pileup

Here, we repeat the top tagging study in Sec. 4.5 in the presence of pileup, again using SoftKiller with a grid parameter $a_{\text{SK}} = 0.5$. In Fig. 17, we show the same ROC curve as in Fig. 9, but with the addition of 140 pileup vertices. As in the previous study without pileup, additional SD grooming layers improve the signal efficiency, with the observables after RSD leading to much better discrimination between top and QCD jets. Here, though, the improvement is much more substantial, since the gains in mass resolution in high-pileup condition is quite dramatic; see Sec. 5.1. This allows for reasonable top tagging performance even with a narrow $m \in [160, 185]$ GeV top window, despite the large pileup multiplicity.

References

- [1] A. Abdesselam et al., *Boosted objects: A Probe of beyond the Standard Model physics*, *Eur. Phys. J. C* **71** (2011) 1661, [[arXiv:1012.5412](#)].
- [2] A. Altheimer et al., *Jet Substructure at the Tevatron and LHC: New results, new tools, new benchmarks*, *J. Phys. G* **39** (2012) 063001, [[arXiv:1201.0008](#)].
- [3] A. Altheimer et al., *Boosted objects and jet substructure at the LHC. Report of BOOST2012, held at IFIC Valencia, 23rd-27th of July 2012*, *Eur. Phys. J. C* **74** (2014), no. 3 2792, [[arXiv:1311.2708](#)].
- [4] D. Adams et al., *Towards an Understanding of the Correlations in Jet Substructure*, *Eur. Phys. J. C* **75** (2015), no. 9 409, [[arXiv:1504.00679](#)].
- [5] M. Cacciari, *Phenomenological and theoretical developments in jet physics at the LHC*, *Int. J. Mod. Phys. A* **30** (2015), no. 31 1546001, [[arXiv:1509.02272](#)].
- [6] A. J. Larkoski, I. Moult, and B. Nachman, *Jet Substructure at the Large Hadron Collider: A Review of Recent Advances in Theory and Machine Learning*, [arXiv:1709.04464](#).
- [7] D. Bhatia, R. Camacho, G. Chachamis, S. Chatterjee, F. Dreyer, D. Kar, P. Loch, I. Moult, B. Nachman, A. Papaefstathiou, T. Samui, A. Siodmok, G. Soyez, and J. Thaler, *Performance versus robustness: Two-prong substructure taggers for the LHC, contribution to the Les Houches 2017: Physics at TeV Colliders Standard Model Working Group Report*, 2018. [arXiv:1803.07977](#).
- [8] M. H. Seymour, *Tagging a heavy Higgs boson*, in *ECFA Large Hadron Collider Workshop, Aachen, Germany, 4-9 Oct 1990: Proceedings.2.*, pp. 557–569, 1991.
- [9] M. H. Seymour, *Searches for new particles using cone and cluster jet algorithms: A Comparative study*, *Z. Phys. C* **62** (1994) 127–138.
- [10] J. M. Butterworth, B. E. Cox, and J. R. Forshaw, *WW scattering at the CERN LHC*, *Phys. Rev. D* **65** (2002) 096014, [[hep-ph/0201098](#)].
- [11] J. M. Butterworth, J. R. Ellis, and A. R. Raklev, *Reconstructing sparticle mass spectra using hadronic decays*, *JHEP* **05** (2007) 033, [[hep-ph/0702150](#)].
- [12] J. M. Butterworth, A. R. Davison, M. Rubin, and G. P. Salam, *Jet substructure as a new Higgs search channel at the LHC*, *Phys. Rev. Lett.* **100** (2008) 242001, [[arXiv:0802.2470](#)].
- [13] J. Thaler and L.-T. Wang, *Strategies to Identify Boosted Tops*, *JHEP* **07** (2008) 092, [[arXiv:0806.0023](#)].

- [14] D. E. Kaplan, K. Rehermann, M. D. Schwartz, and B. Tweedie, *Top Tagging: A Method for Identifying Boosted Hadronically Decaying Top Quarks*, *Phys. Rev. Lett.* **101** (2008) 142001, [[arXiv:0806.0848](#)].
- [15] D. Krohn, J. Thaler, and L.-T. Wang, *Jet Trimming*, *JHEP* **02** (2010) 084, [[arXiv:0912.1342](#)].
- [16] S. D. Ellis, C. K. Vermilion, and J. R. Walsh, *Techniques for improved heavy particle searches with jet substructure*, *Phys. Rev.* **D80** (2009) 051501, [[arXiv:0903.5081](#)].
- [17] S. D. Ellis, C. K. Vermilion, and J. R. Walsh, *Recombination Algorithms and Jet Substructure: Pruning as a Tool for Heavy Particle Searches*, *Phys. Rev.* **D81** (2010) 094023, [[arXiv:0912.0033](#)].
- [18] T. Plehn, G. P. Salam, and M. Spannowsky, *Fat Jets for a Light Higgs*, *Phys. Rev. Lett.* **104** (2010) 111801, [[arXiv:0910.5472](#)].
- [19] J.-H. Kim, *Rest Frame Subjet Algorithm With SIScone Jet For Fully Hadronic Decaying Higgs Search*, *Phys. Rev.* **D83** (2011) 011502, [[arXiv:1011.1493](#)].
- [20] J. Thaler and K. Van Tilburg, *Identifying Boosted Objects with N -subjettiness*, *JHEP* **03** (2011) 015, [[arXiv:1011.2268](#)].
- [21] J. Thaler and K. Van Tilburg, *Maximizing Boosted Top Identification by Minimizing N -subjettiness*, *JHEP* **02** (2012) 093, [[arXiv:1108.2701](#)].
- [22] A. J. Larkoski, G. P. Salam, and J. Thaler, *Energy Correlation Functions for Jet Substructure*, *JHEP* **06** (2013) 108, [[arXiv:1305.0007](#)].
- [23] Y.-T. Chien, *Telescoping jets: Probing hadronic event structure with multiple R s*, *Phys. Rev.* **D90** (2014), no. 5 054008, [[arXiv:1304.5240](#)].
- [24] A. J. Larkoski, I. Moulton, and D. Neill, *Power Counting to Better Jet Observables*, *JHEP* **12** (2014) 009, [[arXiv:1409.6298](#)].
- [25] I. Moulton, L. Necib, and J. Thaler, *New Angles on Energy Correlation Functions*, *JHEP* **12** (2016) 153, [[arXiv:1609.07483](#)].
- [26] I. Feige, M. D. Schwartz, I. W. Stewart, and J. Thaler, *Precision Jet Substructure from Boosted Event Shapes*, *Phys.Rev.Lett.* **109** (2012) 092001, [[arXiv:1204.3898](#)].
- [27] M. Field, G. Gur-Ari, D. A. Kosower, L. Mannelli, and G. Perez, *Three-Prong Distribution of Massive Narrow QCD Jets*, *Phys.Rev.* **D87** (2013), no. 9 094013, [[arXiv:1212.2106](#)].
- [28] M. Dasgupta, A. Fregoso, S. Marzani, and G. P. Salam, *Towards an understanding of jet substructure*, *JHEP* **09** (2013) 029, [[arXiv:1307.0007](#)].
- [29] M. Dasgupta, A. Fregoso, S. Marzani, and A. Powling, *Jet substructure with analytical methods*, *Eur. Phys. J.* **C73** (2013), no. 11 2623, [[arXiv:1307.0013](#)].
- [30] A. J. Larkoski, J. Thaler, and W. J. Waalewijn, *Gaining (Mutual) Information about Quark/Gluon Discrimination*, *JHEP* **1411** (2014) 129, [[arXiv:1408.3122](#)].
- [31] M. Dasgupta, A. Powling, and A. Siodmok, *On jet substructure methods for signal jets*, *JHEP* **08** (2015) 079, [[arXiv:1503.01088](#)].
- [32] M. H. Seymour, *Jet shapes in hadron collisions: Higher orders, resummation and hadronization*, *Nucl. Phys.* **B513** (1998) 269–300, [[hep-ph/9707338](#)].

- [33] H.-n. Li, Z. Li, and C.-P. Yuan, *QCD resummation for jet substructures*, *Phys.Rev.Lett.* **107** (2011) 152001, [[arXiv:1107.4535](#)].
- [34] A. J. Larkoski, *QCD Analysis of the Scale-Invariance of Jets*, *Phys.Rev.* **D86** (2012) 054004, [[arXiv:1207.1437](#)].
- [35] M. Jankowiak and A. J. Larkoski, *Angular Scaling in Jets*, *JHEP* **1204** (2012) 039, [[arXiv:1201.2688](#)].
- [36] Y.-T. Chien and I. Vitev, *Jet Shape Resummation Using Soft-Collinear Effective Theory*, *JHEP* **1412** (2014) 061, [[arXiv:1405.4293](#)].
- [37] Y.-T. Chien, *Resummation of Jet Shapes and Extracting Properties of the Quark-Gluon Plasma*, *Int.J.Mod.Phys.Conf.Ser.* **37** (2015) 1560047, [[arXiv:1411.0741](#)].
- [38] J. Isaacson, H.-n. Li, Z. Li, and C. P. Yuan, *Factorization for substructures of boosted Higgs jets*, [arXiv:1505.06368](#).
- [39] D. Krohn, M. D. Schwartz, T. Lin, and W. J. Waalewijn, *Jet Charge at the LHC*, *Phys.Rev.Lett.* **110** (2013), no. 21 212001, [[arXiv:1209.2421](#)].
- [40] W. J. Waalewijn, *Calculating the Charge of a Jet*, *Phys.Rev.* **D86** (2012) 094030, [[arXiv:1209.3019](#)].
- [41] A. J. Larkoski, I. Moult, and D. Neill, *Toward Multi-Differential Cross Sections: Measuring Two Angularities on a Single Jet*, *JHEP* **1409** (2014) 046, [[arXiv:1401.4458](#)].
- [42] A. J. Larkoski, S. Marzani, G. Soyez, and J. Thaler, *Soft Drop*, *JHEP* **05** (2014) 146, [[arXiv:1402.2657](#)].
- [43] M. Procura, W. J. Waalewijn, and L. Zeune, *Resummation of Double-Differential Cross Sections and Fully-Unintegrated Parton Distribution Functions*, *JHEP* **1502** (2015) 117, [[arXiv:1410.6483](#)].
- [44] D. Bertolini, J. Thaler, and J. R. Walsh, *The First Calculation of Fractional Jets*, *JHEP* **1505** (2015) 008, [[arXiv:1501.01965](#)].
- [45] B. Bhattacharjee, S. Mukhopadhyay, M. M. Nojiri, Y. Sakaki, and B. R. Webber, *Associated jet and subjet rates in light-quark and gluon jet discrimination*, *JHEP* **1504** (2015) 131, [[arXiv:1501.04794](#)].
- [46] A. J. Larkoski, I. Moult, and D. Neill, *Analytic Boosted Boson Discrimination*, *JHEP* **05** (2016) 117, [[arXiv:1507.03018](#)].
- [47] M. Dasgupta, L. Schunk, and G. Soyez, *Jet shapes for boosted jet two-prong decays from first-principles*, *JHEP* **04** (2016) 166, [[arXiv:1512.00516](#)].
- [48] M. Dasgupta, A. Powling, L. Schunk, and G. Soyez, *Improved jet substructure methods: Y-splitter and variants with grooming*, *JHEP* **12** (2016) 079, [[arXiv:1609.07149](#)].
- [49] G. P. Salam, L. Schunk, and G. Soyez, *Dichroic subjettness ratios to distinguish colour flows in boosted boson tagging*, *JHEP* **03** (2017) 022, [[arXiv:1612.03917](#)].
- [50] C. Frye, A. J. Larkoski, M. D. Schwartz, and K. Yan, *Precision physics with pile-up insensitive observables*, [arXiv:1603.06375](#).
- [51] C. Frye, A. J. Larkoski, M. D. Schwartz, and K. Yan, *Factorization for groomed jet substructure beyond the next-to-leading logarithm*, *JHEP* **07** (2016) 064, [[arXiv:1603.09338](#)].

- [52] Z.-B. Kang, F. Ringer, and I. Vitev, *Jet substructure using semi-inclusive jet functions in SCET*, *JHEP* **11** (2016) 155, [[arXiv:1606.07063](#)].
- [53] A. Hornig, Y. Makris, and T. Mehen, *Jet Shapes in Dijet Events at the LHC in SCET*, *JHEP* **04** (2016) 097, [[arXiv:1601.01319](#)].
- [54] S. Marzani, L. Schunk, and G. Soyez, *A study of jet mass distributions with grooming*, *JHEP* **07** (2017) 132, [[arXiv:1704.02210](#)].
- [55] S. Marzani, L. Schunk, and G. Soyez, *The jet mass distribution after Soft Drop*, *Eur. Phys. J. C* **78** (2018), no. 2 96, [[arXiv:1712.05105](#)].
- [56] Y.-T. Chien, A. Emerman, S.-C. Hsu, S. Meehan, and Z. Montague, *Telescoping jet substructure*, [arXiv:1711.11041](#).
- [57] Y.-T. Chien and R. Kunnawalkam Elayavalli, *Probing heavy ion collisions using quark and gluon jet substructure*, [arXiv:1803.03589](#).
- [58] CMS Collaboration, S. Chatrchyan et al., *Studies of jet mass in dijet and $W/Z + \text{jet}$ events*, *JHEP* **05** (2013) 090, [[arXiv:1303.4811](#)].
- [59] ATLAS Collaboration, G. Aad et al., *Performance of jet substructure techniques for large- R jets in proton-proton collisions at $\sqrt{s} = 7$ TeV using the ATLAS detector*, *JHEP* **09** (2013) 076, [[arXiv:1306.4945](#)].
- [60] CMS Collaboration, V. Khachatryan et al., *Identification techniques for highly boosted W bosons that decay into hadrons*, *JHEP* **12** (2014) 017, [[arXiv:1410.4227](#)].
- [61] CMS Collaboration, S. Chatrchyan et al., *Search for a Higgs boson in the decay channel $H \rightarrow ZZ(*) \rightarrow q \bar{q} \ell^- \ell^+$ in pp collisions at $\sqrt{s} = 7$ TeV*, *JHEP* **1204** (2012) 036, [[arXiv:1202.1416](#)].
- [62] CMS Collaboration, *Search for a Standard Model-like Higgs boson decaying into WW to $l \nu q \bar{q}$ in pp collisions at $\sqrt{s} = 8$ TeV*, Tech. Rep. CMS-PAS-HIG-13-008, 2013.
- [63] ATLAS Collaboration, G. Aad et al., *Measurement of jet charge in dijet events from $\sqrt{s} = 8$ TeV pp collisions with the ATLAS detector*, *Phys. Rev. D* **93** (2016), no. 5 052003, [[arXiv:1509.05190](#)].
- [64] ATLAS Collaboration, G. Aad et al., *Measurement of colour flow with the jet pull angle in $t\bar{t}$ events using the ATLAS detector at $\sqrt{s} = 8$ TeV*, *Phys. Lett. B* **750** (2015) 475–493, [[arXiv:1506.05629](#)].
- [65] *Performance of jet substructure techniques in early $\sqrt{s} = 13$ TeV pp collisions with the ATLAS detector*, Tech. Rep. ATLAS-CONF-2015-035, CERN, Geneva, Aug, 2015.
- [66] ATLAS Collaboration, G. Aad et al., *Identification of boosted, hadronically decaying W bosons and comparisons with ATLAS data taken at $\sqrt{s} = 8$ TeV*, *Eur. Phys. J. C* **76** (2016), no. 3 154, [[arXiv:1510.05821](#)].
- [67] ATLAS Collaboration, G. Aad et al., *Measurement of the differential cross-section of highly boosted top quarks as a function of their transverse momentum in $\sqrt{s} = 8$ TeV proton-proton collisions using the ATLAS detector*, *Phys. Rev. D* **93** (2016), no. 3 032009, [[arXiv:1510.03818](#)].
- [68] *Studies of b -tagging performance and jet substructure in a high p_T $g \rightarrow b\bar{b}$ rich sample of large- R jets from pp collisions at $\sqrt{s} = 8$ TeV with the ATLAS detector*, Tech. Rep. ATLAS-CONF-2016-002, CERN, Geneva, Feb, 2016.

- [69] **ATLAS Collaboration** Collaboration, *Boosted Higgs ($\rightarrow b\bar{b}$) Boson Identification with the ATLAS Detector at $\sqrt{s} = 13$ TeV*, Tech. Rep. ATLAS-CONF-2016-039, CERN, Geneva, Aug, 2016.
- [70] **ATLAS Collaboration** Collaboration, *Discrimination of Light Quark and Gluon Jets in pp collisions at $\sqrt{s} = 8$ TeV with the ATLAS Detector*, Tech. Rep. ATLAS-CONF-2016-034, CERN, Geneva, Jul, 2016.
- [71] **CMS Collaboration** Collaboration, *Measurement of the $t\bar{t}$ production cross section at 13 TeV in the all-jets final state*, Tech. Rep. CMS-PAS-TOP-16-013, CERN, Geneva, 2016.
- [72] **CMS Collaboration** Collaboration, *Search for $t\bar{t}H$ production in the $H \rightarrow b\bar{b}$ decay channel with $\sqrt{s} = 13$ TeV pp collisions at the CMS experiment*, Tech. Rep. CMS-PAS-HIG-16-004, CERN, Geneva, 2016.
- [73] **CMS Collaboration**, *Search for BSM $t\bar{t}$ Production in the Boosted All-Hadronic Final State*, Tech. Rep. CMS-PAS-EXO-11-006, 2011.
- [74] **ATLAS, CMS Collaboration**, S. Fleischmann, *Boosted top quark techniques and searches for $t\bar{t}$ resonances at the LHC*, *J.Phys.Conf.Ser.* **452** (2013), no. 1 012034.
- [75] **ATLAS, CMS Collaboration**, J. Pilot, *Boosted Top Quarks, Top Pair Resonances, and Top Partner Searches at the LHC*, *EPJ Web Conf.* **60** (2013) 09003.
- [76] **ATLAS Collaboration**, *Performance of boosted top quark identification in 2012 ATLAS data*, Tech. Rep. ATLAS-CONF-2013-084, ATLAS-COM-CONF-2013-074, 2013.
- [77] **CMS Collaboration**, S. Chatrchyan et al., *Search for Anomalous $t\bar{t}$ Production in the Highly-Boosted All-Hadronic Final State*, *JHEP* **1209** (2012) 029, [[arXiv:1204.2488](#)].
- [78] **CMS Collaboration** Collaboration, *Search for pair-produced vector-like quarks of charge $-1/3$ decaying to bH using boosted Higgs jet-tagging in pp collisions at $\sqrt{s} = 8$ TeV*, Tech. Rep. CMS-PAS-B2G-14-001, CERN, Geneva, 2014.
- [79] **CMS Collaboration** Collaboration, *Search for top-Higgs resonances in all-hadronic final states using jet substructure methods*, Tech. Rep. CMS-PAS-B2G-14-002, CERN, Geneva, 2014.
- [80] **CMS Collaboration**, V. Khachatryan et al., *Search for vector-like T quarks decaying to top quarks and Higgs bosons in the all-hadronic channel using jet substructure*, *JHEP* **06** (2015) 080, [[arXiv:1503.01952](#)].
- [81] **CMS Collaboration**, V. Khachatryan et al., *Search for a massive resonance decaying into a Higgs boson and a W or Z boson in hadronic final states in proton-proton collisions at $\sqrt{s} = 8$ TeV*, *JHEP* **02** (2016) 145, [[arXiv:1506.01443](#)].
- [82] **ATLAS Collaboration**, G. Aad et al., *Search for high-mass diboson resonances with boson-tagged jets in proton-proton collisions at $\sqrt{s} = 8$ TeV with the ATLAS detector*, *JHEP* **12** (2015) 055, [[arXiv:1506.00962](#)].
- [83] **ATLAS Collaboration**, M. Aaboud et al., *Searches for heavy diboson resonances in pp collisions at $\sqrt{s} = 13$ TeV with the ATLAS detector*, *JHEP* **09** (2016) 173, [[arXiv:1606.04833](#)].
- [84] **ATLAS Collaboration**, M. Aaboud et al., *Search for heavy resonances decaying to a Z boson and a photon in pp collisions at $\sqrt{s} = 13$ TeV with the ATLAS detector*, *Phys. Lett. B* **764** (2017) 11–30, [[arXiv:1607.06363](#)].

- [85] **ATLAS Collaboration**, M. Aaboud et al., *Search for dark matter produced in association with a hadronically decaying vector boson in pp collisions at $\sqrt{s} = 13$ TeV with the ATLAS detector*, *Phys. Lett.* **B763** (2016) 251–268, [[arXiv:1608.02372](#)].
- [86] **ATLAS Collaboration**, *Search for resonances with boson-tagged jets in 15.5 fb^{-1} of pp collisions at $\sqrt{s} = 13$ TeV collected with the ATLAS detector*, Tech. Rep. ATLAS-CONF-2016-055, CERN, Geneva, Aug, 2016.
- [87] *Search for diboson resonances in the llqq final state in pp collisions at $\sqrt{s} = 13$ TeV with the ATLAS detector*, Tech. Rep. ATLAS-CONF-2015-071, CERN, Geneva, Dec, 2015.
- [88] *Search for diboson resonances in the $\nu\nu q\bar{q}$ final state in pp collisions at $\sqrt{s} = 13$ TeV with the ATLAS detector*, Tech. Rep. ATLAS-CONF-2015-068, CERN, Geneva, Dec, 2015.
- [89] **CMS Collaboration**, *Search for dark matter in final states with an energetic jet, or a hadronically decaying W or Z boson using 12.9 fb^{-1} of data at $\sqrt{s} = 13$ TeV*, Tech. Rep. CMS-PAS-EXO-16-037, CERN, Geneva, 2016.
- [90] **CMS Collaboration**, *Search for new physics in a boosted hadronic monotop final state using 12.9 fb^{-1} of $\sqrt{s} = 13$ TeV data*, Tech. Rep. CMS-PAS-EXO-16-040, CERN, Geneva, 2016.
- [91] **CMS Collaboration**, V. Khachatryan et al., *Search for dark matter in proton-proton collisions at 8 TeV with missing transverse momentum and vector boson tagged jets*, *Submitted to: JHEP* (2016) [[arXiv:1607.05764](#)].
- [92] **CMS Collaboration**, *Searches for invisible Higgs boson decays with the CMS detector.*, Tech. Rep. CMS-PAS-HIG-16-016, CERN, Geneva, 2016.
- [93] **CMS Collaboration**, *Search for top quark-antiquark resonances in the all-hadronic final state at $\sqrt{s} = 13$ TeV*, Tech. Rep. CMS-PAS-B2G-15-003, CERN, Geneva, 2016.
- [94] **CMS Collaboration**, *Search for dark matter in association with a boosted top quark in the all hadronic final state*, Tech. Rep. CMS-PAS-EXO-16-017, CERN, Geneva, 2016.
- [95] Y. L. Dokshitzer, G. D. Leder, S. Moretti, and B. R. Webber, *Better jet clustering algorithms*, *JHEP* **08** (1997) 001, [[hep-ph/9707323](#)].
- [96] M. Wobisch and T. Wengler, *Hadronization corrections to jet cross-sections in deep inelastic scattering*, in *Monte Carlo generators for HERA physics. Proceedings, Workshop, Hamburg, Germany, 1998-1999*, pp. 270–279, 1998. [[hep-ph/9907280](#)].
- [97] **CMS Collaboration**, *Measurement of the differential jet production cross section with respect to jet mass and transverse momentum in dijet events from pp collisions at $\sqrt{s} = 13$ TeV*, Tech. Rep. CMS-PAS-SMP-16-010, CERN, Geneva, 2017.
- [98] **ATLAS Collaboration**, M. Aaboud et al., *A measurement of the soft-drop jet mass in pp collisions at $\sqrt{s} = 13$ TeV with the ATLAS detector*, [[arXiv:1711.08341](#)].
- [99] **CMS Collaboration**, A. M. Sirunyan et al., *Search for Low Mass Vector Resonances Decaying to Quark-Antiquark Pairs in Proton-Proton Collisions at $\sqrt{s} = 13$ TeV*, *Phys. Rev. Lett.* **119** (2017), no. 11 111802, [[arXiv:1705.10532](#)].
- [100] **ATLAS Collaboration**, M. Aaboud et al., *Search for diboson resonances with boson-tagged jets in pp collisions at $\sqrt{s} = 13$ TeV with the ATLAS detector*, *Phys. Lett.* **B777** (2018) 91–113, [[arXiv:1708.04445](#)].

- [101] CMS Collaboration, A. M. Sirunyan et al., *Search for a heavy resonance decaying into a Z boson and a vector boson in the $\nu\bar{\nu}q\bar{q}$ final state*, [arXiv:1803.03838](#).
- [102] CMS Collaboration, A. M. Sirunyan et al., *Search for dark matter in events with energetic, hadronically decaying top quarks and missing transverse momentum at $\sqrt{s} = 13$ TeV*, [arXiv:1801.08427](#).
- [103] CMS Collaboration, A. M. Sirunyan et al., *Inclusive search for a highly boosted Higgs boson decaying to a bottom quark-antiquark pair*, *Phys. Rev. Lett.* **120** (2018), no. 7 071802, [[arXiv:1709.05543](#)].
- [104] A. Larkoski, S. Marzani, J. Thaler, A. Tripathy, and W. Xue, *Exposing the QCD Splitting Function with CMS Open Data*, *Phys. Rev. Lett.* **119** (2017), no. 13 132003, [[arXiv:1704.05066](#)].
- [105] A. Tripathy, W. Xue, A. Larkoski, S. Marzani, and J. Thaler, *Jet Substructure Studies with CMS Open Data*, *Phys. Rev.* **D96** (2017), no. 7 074003, [[arXiv:1704.05842](#)].
- [106] CMS Collaboration, A. M. Sirunyan et al., *Measurement of the splitting function in pp and PbPb collisions at $\sqrt{s_{NN}} = 5.02$ TeV*, [arXiv:1708.09429](#).
- [107] ALICE Collaboration, D. Caffarri, *Exploring jet substructure with jet shapes in ALICE*, *Nucl. Phys.* **A967** (2017) 528–531, [[arXiv:1704.05230](#)].
- [108] STAR Collaboration, K. Kauder, *Measurement of the Shared Momentum Fraction z_g using Jet Reconstruction in p+p and Au+Au Collisions with STAR*, *Nucl. Phys.* **A967** (2017) 516–519, [[arXiv:1704.03046](#)].
- [109] Y.-T. Chien and I. Vitev, *Probing the hardest branching of jets in heavy ion collisions*, *Phys. Rev. Lett.* **119** (2017), no. 11 112301, [[arXiv:1608.07283](#)].
- [110] J. G. Milhano, U. A. Wiedemann, and K. C. Zapp, *Sensitivity of jet substructure to jet-induced medium response*, [arXiv:1707.04142](#).
- [111] Y. Mehtar-Tani and K. Tywoniuk, *Groomed jets in heavy-ion collisions: sensitivity to medium-induced bremsstrahlung*, *JHEP* **04** (2017) 125, [[arXiv:1610.08930](#)].
- [112] M. Cacciari, G. P. Salam, and G. Soyez, *The Catchment Area of Jets*, *JHEP* **04** (2008) 005, [[arXiv:0802.1188](#)].
- [113] M. Cacciari, G. P. Salam, and G. Soyez, *SoftKiller, a particle-level pileup removal method*, *Eur. Phys. J.* **C75** (2015), no. 2 59, [[arXiv:1407.0408](#)].
- [114] M. Cacciari and G. P. Salam, *Pileup subtraction using jet areas*, *Phys. Lett.* **B659** (2008) 119–126, [[arXiv:0707.1378](#)].
- [115] A. J. Larkoski and J. Thaler, *Unsafe but Calculable: Ratios of Angularities in Perturbative QCD*, *JHEP* **09** (2013) 137, [[arXiv:1307.1699](#)].
- [116] A. J. Larkoski, S. Marzani, and J. Thaler, *Sudakov Safety in Perturbative QCD*, *Phys. Rev.* **D91** (2015), no. 11 111501, [[arXiv:1502.01719](#)].
- [117] C. Frye, A. J. Larkoski, J. Thaler, and K. Zhou, *Casimir Meets Poisson: Improved Quark/Gluon Discrimination with Counting Observables*, [arXiv:1704.06266](#).
- [118] “Fastjet contrib.” <http://fastjet.hepforge.org/contrib/>.
- [119] T. Sjostrand, S. Mrenna, and P. Z. Skands, *PYTHIA 6.4 Physics and Manual*, *JHEP* **05** (2006) 026, [[hep-ph/0603175](#)].

- [120] T. Sjostrand, S. Mrenna, and P. Z. Skands, *A Brief Introduction to PYTHIA 8.1*, *Comput. Phys. Commun.* **178** (2008) 852–867, [[arXiv:0710.3820](#)].
- [121] T. Sjostrand, S. Ask, J. R. Christiansen, R. Corke, N. Desai, P. Ilten, S. Mrenna, S. Prestel, C. O. Rasmussen, and P. Z. Skands, *An Introduction to PYTHIA 8.2*, *Comput. Phys. Commun.* **191** (2015) 159–177, [[arXiv:1410.3012](#)].
- [122] G. Soyez, *Pileup mitigation at the LHC: a theorist’s view*. Habilitation thesis, Université Pierre et Marie Curie, and IPhT, CEA Saclay, 2018. [arXiv:1801.09721](#).
- [123] M. Cacciari, G. P. Salam, and G. Soyez, *FastJet User Manual*, *Eur. Phys. J.* **C72** (2012) 1896, [[arXiv:1111.6097](#)].
- [124] M. Cacciari, G. P. Salam, and G. Soyez, *The Anti- $k(t)$ jet clustering algorithm*, *JHEP* **04** (2008) 063, [[arXiv:0802.1189](#)].
- [125] J. Tseng and H. Evans, *Sequential recombination algorithm for jet clustering and background subtraction*, *Phys. Rev.* **D88** (2013) 014044, [[arXiv:1304.1025](#)].
- [126] D. Duffy and Z. Sullivan, *A priority based noise tolerant jet framework and algorithm*, [arXiv:1606.04497](#).
- [127] **ATLAS** Collaboration, G. Aad et al., *Performance of pile-up mitigation techniques for jets in pp collisions at $\sqrt{s} = 8$ TeV using the ATLAS detector*, *Eur. Phys. J.* **C76** (2016), no. 11 581, [[arXiv:1510.03823](#)].
- [128] M. Dasgupta and G. P. Salam, *Resummation of nonglobal QCD observables*, *Phys. Lett.* **B512** (2001) 323–330, [[hep-ph/0104277](#)].
- [129] M. Dasgupta and G. P. Salam, *Accounting for coherence in interjet $E(t)$ flow: A Case study*, *JHEP* **03** (2002) 017, [[hep-ph/0203009](#)].
- [130] A. H. Hoang, S. Mantry, A. Pathak, and I. W. Stewart, *Extracting a Short Distance Top Mass with Light Grooming*, [arXiv:1708.02586](#).
- [131] S. Y. Choi, D. J. Miller, M. M. Muhlleitner, and P. M. Zerwas, *Identifying the Higgs spin and parity in decays to Z pairs*, *Phys. Lett.* **B553** (2003) 61–71, [[hep-ph/0210077](#)].
- [132] N. T. Meyer and K. Desch, *Determining resonance parameters of heavy Higgs bosons at a future linear collider*, *Eur. Phys. J.* **C35** (2004) 171–176.
- [133] F. Bishara, R. Contino, and J. Rojo, *Higgs pair production in vector-boson fusion at the LHC and beyond*, *Eur. Phys. J.* **C77** (2017), no. 7 481, [[arXiv:1611.03860](#)].
- [134] G. Soyez, G. P. Salam, J. Kim, S. Dutta, and M. Cacciari, *Pileup subtraction for jet shapes*, *Phys. Rev. Lett.* **110** (2013), no. 16 162001, [[arXiv:1211.2811](#)].
- [135] **CMS** Collaboration, *Particle-Flow Event Reconstruction in CMS and Performance for Jets, T_{aus} , and MET*, .
- [136] D. Bertolini, P. Harris, M. Low, and N. Tran, *Pileup Per Particle Identification*, *JHEP* **10** (2014) 059, [[arXiv:1407.6013](#)].
- [137] P. T. Komiske, E. M. Metodiev, B. Nachman, and M. D. Schwartz, *Pileup Mitigation with Machine Learning (PUMML)*, *JHEP* **12** (2017) 051, [[arXiv:1707.08600](#)].
- [138] A. Banfi, G. P. Salam, and G. Zanderighi, *Principles of general final-state resummation and automated implementation*, *JHEP* **03** (2005) 073, [[hep-ph/0407286](#)].

- [139] A. Banfi, H. McAslan, P. F. Monni, and G. Zanderighi, *A general method for the resummation of event-shape distributions in e^+e^- annihilation*, *JHEP* **05** (2015) 102, [[arXiv:1412.2126](#)].
- [140] A. Banfi, H. McAslan, P. F. Monni, and G. Zanderighi, *The two-jet rate in e^+e^- at next-to-next-to-leading-logarithmic order*, *Phys. Rev. Lett.* **117** (2016), no. 17 172001, [[arXiv:1607.03111](#)].
- [141] C. W. Bauer, S. Fleming, D. Pirjol, and I. W. Stewart, *An Effective field theory for collinear and soft gluons: Heavy to light decays*, *Phys. Rev.* **D63** (2001) 114020, [[hep-ph/0011336](#)].
- [142] C. W. Bauer and I. W. Stewart, *Invariant operators in collinear effective theory*, *Phys. Lett.* **B516** (2001) 134–142, [[hep-ph/0107001](#)].
- [143] C. W. Bauer, D. Pirjol, and I. W. Stewart, *Soft collinear factorization in effective field theory*, *Phys. Rev.* **D65** (2002) 054022, [[hep-ph/0109045](#)].
- [144] C. W. Bauer, S. Fleming, D. Pirjol, I. Z. Rothstein, and I. W. Stewart, *Hard scattering factorization from effective field theory*, *Phys. Rev.* **D66** (2002) 014017, [[hep-ph/0202088](#)].
- [145] S. Catani and M. H. Seymour, *The Dipole formalism for the calculation of QCD jet cross-sections at next-to-leading order*, *Phys. Lett.* **B378** (1996) 287–301, [[hep-ph/9602277](#)].
- [146] S. Catani and M. H. Seymour, *A General algorithm for calculating jet cross-sections in NLO QCD*, *Nucl. Phys.* **B485** (1997) 291–419, [[hep-ph/9605323](#)]. [Erratum: Nucl. Phys.B510,503(1998)].